PHILOSOPHICAL TRANSACTIONS OF THE ROYAL SOCIETY A MATHEMATICAL, PHYSICAL & ENGINEERING SCIENCES

The Application of a Pulsed-Light Rangefinder (Lidar) to the Study of Chimney Plumes

P. M. Hamilton

Phil. Trans. R. Soc. Lond. A 1969 **265**, 153-172
doi: 10.1098/rsta.1969.0044

Phil. Trans. Roy. Soc. Lond. A. **265**, 153–172 (1969) [153]
Printed in Great Britain

The application of a pulsed-light rangefinder (lidar) to the study of chimney plumes

By P. M. Hamilton
Central Electricity Research Laboratories, Kelvin Avenue, Leatherhead, Surrey

[Plates 1 and 2]

Lidar observations, depending on the detection of backscatter from a pulse of light by particles along its path, have been used to study chimney plumes and their environment. Important technical improvements to the basic equipment have included the use of swept gain and the development of a brightness modulated display. A number of examples of lidar scans through plumes are presented to demonstrate the value of the improved display.

Lidar observations of plumes over periods of about an hour have been used to predict the concentration of pollution at the ground. In neutral conditions, the predictions were significantly better than predictions based only on meteorological data. Observations of the rise and growth of a plume have suggested that, in the equation of motion describing the rise of a plume element, the rate of change of upward momentum should be equated to about one-half rather than the whole of the buoyancy force.

Finally, a technique of analysis leading to vertical profiles of aerosol concentration in the lower layers of the atmosphere is outlined. These profiles often reveal features that are vital to a full understanding of plume behaviour.

1. Introduction

Following the development of the pulsed laser, lidar has become firmly established as an important tool in the study of the atmosphere. The detection of the radiation scattered from the laser pulse as it travels through the atmosphere has enabled the air pollution meteorologist to measure remotely the distribution and dispersion of atmospheric aerosols. For the past three years, a ruby laser lidar has been used by the Central Electricity Research Laboratories (C.E.R.L.) to study the behaviour of power station chimney plumes, and the purpose of this paper is to survey the techniques that have been developed during this period. By way of illustration, a few of the measurements that have been obtained will also be presented.

2. Lidar performance

The equations from which the performance of a lidar may be calculated have been developed by, among others, Collis (1966), Northend, Honey & Evans (1966) and Barrett & Ben-Dov (1967). The radiation scattered back from the laser pulse and received after its journey to and from an atmospheric target is given by the so-called lidar equation:

$$S(r) = \frac{G}{r^2}\,\beta'(r)\exp\left[-2\int_0^r \sigma(r')\,\mathrm{d}r'\right], \tag{1}$$

where

$$G = (c/8\pi)\,JA. \tag{2}$$

In these equations

S is the power received from a target (W),
r is the range of the target (m),
G is the system sensitivity (W m),
β' is the volume backscattering coefficient of the target (m^{-1}),
$\sigma(r')$ is the coefficient of extinction of the atmosphere at range r' (m^{-1}),

c is the velocity of light (3.0×10^8 m s^{-1}),
J is the energy in the transmitted pulse (J),
A is the effective receiver area, allowing for optical system efficiencies (m^2).

If the received power exceeds the minimum detectable signal, then its intensity provides a means of measuring the backscattering and extinction coefficients. The minimum detectable signal is determined by the noise, which includes: (i) the external noise, arising from the incidence of radiation at the detector both from lidar scattering and from the background; and (ii) the internal noise, arising from fluctuations in the detector dark current and thermal noise in the detector load resistor. In the case of a lidar based on a ruby laser source and used in air pollution studies it is usually the external noise which limits performance.

The external noise arises from fluctuations in the emission rate of the photoelectrons resulting from the incidence on the detector of both signal and background radiation. The power received from the background radiation is given by

$$B = \Omega \Delta\lambda A E_\lambda, \tag{3}$$

where

B is the power received from the background (W),
Ω is the receiver field of view (sr),
$\Delta\lambda$ is the optical filter bandpass (nm),
E_λ is the background radiance (W m^{-2} sr^{-1} nm^{-1}).

It is convenient to discuss lidar performance in terms of the emission of photoelectrons at the detector. The rates of emission due to both signal and background radiation are given by

$$n_S = (\lambda/hc)\, qS, \tag{4}$$

$$n_B = (\lambda/hc)\, qB, \tag{5}$$

where

n_S is the photoelectron emission rate due to signal radiation (s^{-1}),
n_B is that due to background radiation (s^{-1})
λ is the wavelength (m),
h is the Planck constant (6.6×10^{-34} J s),
q is the detector quantum efficiency or electron yield per incident photon.

The intensity of noise depends on the sampling interval which, in turn, is determined by the required resolution in range. Taking a sampling interval τ the mean signal and noise counts in each interval are given by

$$\text{signal count} = n_S \tau, \tag{6}$$

$$\text{noise count} = (n_S \tau + n_B \tau)^{\frac{1}{2}}. \tag{7}$$

The equations reviewed above can now be used to describe the performance of a meteorological lidar. This is, perhaps, best done graphically in the manner of figure 1, which is based on the parameters of the C.E.R.L. lidar given in table 1. The curves in the figure were calculated from equation (1) and give the received power as a function of the visual range V, for various values of the target range. They assume a uniform atmosphere in which the volume backscattering coefficient and extinction coefficient vary with the visual range in the way given in table 2. The variation (see table 2) of extinction coefficient with visual range follows Middleton (1952). The visual range and visual extinction coefficient are related through the familiar Koschmieder relation, $V\sigma_{\text{vis}} = 3.9$, where the value of the constant is based on a threshold contrast of 0.02. The ratio of the extinction at the ruby wavelength (694.3 nm) to the visual extinction coefficient

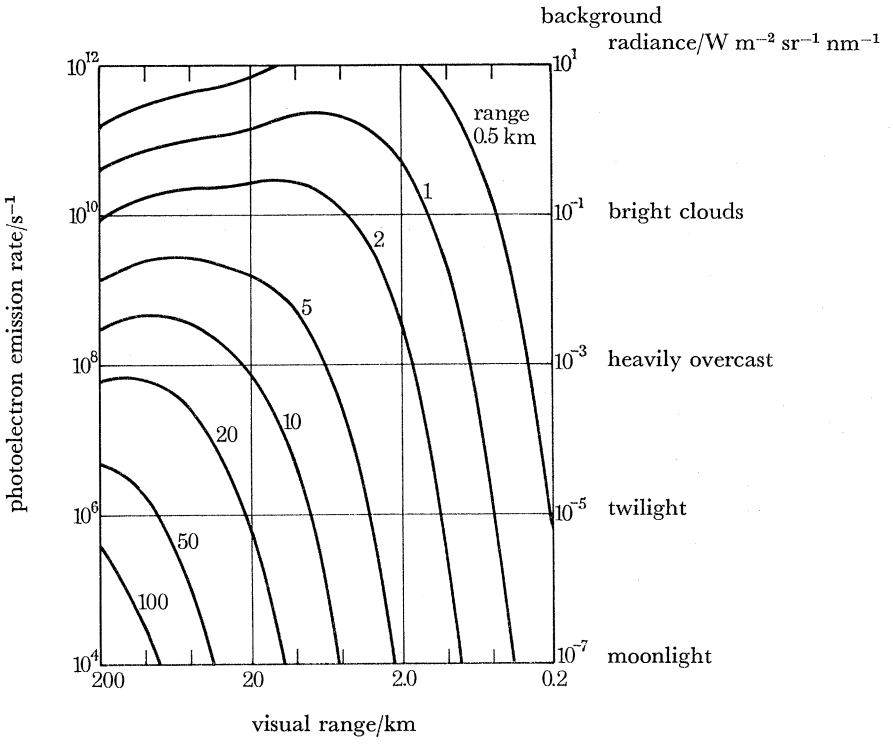

FIGURE 1. Lidar signal from atmospheric backscatter as a function of the visual range with target range as parameter.

TABLE 1. PARAMETERS OF THE CENTRAL ELECTRICITY RESEARCH LABORATORIES LIDAR

output energy (J)	2.0×10^{-1} J
effective receiver area (A) (0.2 m diameter mirror, optical efficiency 0.29)	1.1×10^{-2} m^2
receiver field of view (Ω) (whole angle 5 mrad)	2.0×10^{-5} sr
optical filter bandpass ($\Delta\lambda$)	5.5 nm

TABLE 2. BACKSCATTER AND EXTINCTION COEFFICIENTS AT THE RUBY WAVELENGTH

visual range, v/km	visual extinction coeff., σ_{vis}/m^{-1}	σ/σ_{vis}	extinction coeff., σ/m^{-1}	β'/σ	backscatter coeff., β'/m^{-1}
0.2	2.0×10^{-2}	1.00	2.0×10^{-2}	0.5	1.0×10^{-2}
0.5	7.8×10^{-3}	1.00	7.8×10^{-3}	0.5	3.9×10^{-3}
1.0	3.9×10^{-3}	1.00	3.9×10^{-3}	0.5	2.0×10^{-3}
2.0	2.0×10^{-3}	0.96	1.9×10^{-3}	0.5	1.0×10^{-3}
5.0	7.8×10^{-4}	0.92	7.2×10^{-4}	0.5	3.6×10^{-4}
10	3.9×10^{-4}	0.88	3.4×10^{-4}	0.5	1.7×10^{-4}
20	2.0×10^{-4}	0.84	1.6×10^{-4}	0.5	8.0×10^{-5}
50	7.8×10^{-5}	0.78	6.1×10^{-5}	0.8	4.9×10^{-5}
100	3.9×10^{-5}	0.72	2.8×10^{-5}	1.1	3.1×10^{-5}
200	2.0×10^{-5}	0.60	1.2×10^{-5}	1.3	1.6×10^{-5}
(clear air, 1013.2 mbar, 0 °C)					
330	1.2×10^{-5}	0.40	4.7×10^{-6}	1.5	7.0×10^{-6}

is also taken from Middleton (p. 43). Values of the ratio of the backscatter and extinction coefficients are derived from measurements and calculations by Foitzik & Zschaeck (1953), Collis (1966), Barrett & Ben-Dov (1967), Twomey & Howell (1965) and Waldram (1945*a*, *b*).

The ratio is unity for isotropic scattering. In the atmosphere it ranges from about 0.5 for Mie scattering by the relatively large particles present in conditions of poor visibility to 1.5 for Rayleigh scattering in clear air. Since the ratio depends on the composition and size distribution of the atmospheric aerosol, the values given in table 2 can be no more than a guide. On any given occasion, the ratio may depart from the listed value by a factor two or more, although this does not alter the main conclusions of the present discussion. At this point it is, however, worth mentioning that it is assumed that the intense water vapour absorption lines near 694.215 nm are avoided by keeping the temperature of the ruby outside the range 10 to 15 °C.

Returning to figure 1, the ordinate of received power has been expressed in terms of the photoelectron emission rate, assuming that the energy of a photon at the ruby wavelength is 2.9×10^{-19} J and that the quantum efficiency of the EMI 9558 A photomultiplier detector is 0.03. The values of background radiance which would yield the counts in the ordinate scale are given at the right of the figure. Thus, for example, a radiance of 10^{-1} W m^{-2} sr^{-1} nm^{-1} from a bright cloud would produce a background emission of 10^{10} s^{-1}. If the visual range were 5 km, a similar signal count would be produced by scatter from the atmosphere at a range of 2 km.

The maximum range from which a signal can be detected depends on the ratio of signal to noise counts taken to define the minimum detectable signal. For the purpose of comparison it is convenient to take a ratio of unity, though the value is in reality very much dependent on the type of measurement being made. Equating the signal and noise counts in (6) and (7) and solving for $(n_S\tau)_{\min}$ gives

$$(n_S\tau)_{\min} = \tfrac{1}{2} + (\tfrac{1}{4} + n_B\tau)^{\frac{1}{2}}, \tag{8}$$

or

$$(n_S\tau)_{\min} \approx 1 + (n_B\tau)^{\frac{1}{2}}. \tag{9}$$

Returning to the example of figure 1, a realistic sampling period is 10^{-7} s which gives a resolution of 15 m in range. In the absence of background radiation, the minimum detectable signal is then given by an emission rate of 10^7 s^{-1}. The maximum range from which lidar scatter can be detected in these conditions increases steadily with the meteorological range, though at a decreasing rate. With a visibility of 0.2 km the maximum range is about 0.4 km, at 5 km it is 6 km, and in very clear air with visibility 200 km it is about 40 km. In the case of a fairly bright cloud background producing an emission rate 10^{10} s^{-1}, the mean count in each interval is 10^3, and a barely detectable signal is produced by a mean signal count of $10^{1.5}$ at an emission rate of $10^{8.5}$ s^{-1}. The corresponding values of maximum range at visibilities of 0.2, 5 and 200 km are 0.3, 4 and 10 km respectively. Evidently performance has not deteriorated significantly in conditions of poor visibility, though it has become much worse in clear conditions. By the same token, although performance can usefully be improved in clear conditions by increasing the laser output energy or using a larger collecting mirror, such improvements are very dearly bought in conditions of poor visibility.

Although figure 1 gives the maximum range at which scattering from the free air can be detected it can also be used to estimate the performance of lidar in detecting the enhanced scattering due to smoke plumes. In the present work, scattering from the free air has consistently been detected at ranges of 3 km with a visibility of at least 5 km, suggesting a practical signal/noise ratio of four for the detection of the environmental scatter. In these conditions, enhanced scatter a factor two greater can certainly be detected. This corresponds to a plume within which the visual range is of the order of 2.5 km.

3. Range normalization

It can be seen from the lidar equation (1) that, in the absence of extinction, the signal due to radiation scattered back from the laser pulse varies inversely as the square of range. The signal will decrease even more rapidly if there is significant extinction. A typical lidar oscilloscope trace showing the characteristic decrease of signal with range is shown in figure 2*a*, plate 1. This was taken with the lidar at a low angle of elevation on an occasion when there was a light haze. It is immediately obvious that the rapid decrease of signal with range badly limits the effective dynamic range of the lidar, in the sense that the same range of signals cannot be accommodated at all distances. On the occasion of figure 2*a*, signals ranging from environmental scatter up to only about four times that value can be measured at a distance of 1 km, while, at 2 km, the overall range is a factor 40. In consequence, the accuracy with which the environmental backscatter can be measured is very poor at the greater distances and small variations in it cannot be detected.

It is evidently desirable that this variation in performance with distance be eliminated or, at least, reduced and this has been achieved in the C.E.R.L. lidar by the use of swept receiver gain. The scattered radiation is detected by a photomultiplier whose gain is increased as a function of time in such a way that the output signal remains more or less constant with distance. The upper trace in figure 2*b* shows the effect of using this technique. It was obtained on the same occasion as that of figure 2*a*.

The gain of the photomultiplier was the same in both cases at a distance of 750 m. The swept gain has produced a fairly uniform signal from 300 m to 3 km. Because of the separation of the lidar transmitter and receiver the laser pulse only falls completely within the receiver field of view beyond 300 m and, closer than this, the observed signal must be corrected for this effect.

The application of swept gain to a lidar system was first described by Kaplan & Daly (1967) and the particular circuit used in the present instrument has been outlined by Cohen (1968). Essentially, at the instant of firing, a voltage step is applied to the grid of a triode whose anode provides the photomultiplier supply voltage. The rate of rise of this supply voltage is determined by the magnitude of the voltage step and the time constants of the anode load and a cathode decoupling circuit. With this circuit, the variation of gain as the square of range can be approximated over the interval 300 m to 7.5 km with an accuracy of $\pm 25\%$ and the gain is reproducible within $\pm 5\%$. In practice, on any given occasion, the gain variation is adjusted by trial and error to produce a nearly constant signal over the range of interest. On the occasion of figure 2*b*, the photomultiplier current gain was increased 32 dB in the interval 300 m to 3 km by applying the voltage shown in figure 2*c*. The environmental backscatter decreased by a similar amount, of which 20 dB was due to inverse square law decrease and the remainder to extinction in the light haze.

One undesirable consequence of using swept gain is that the signal due to the background radiance also increases during the sweep. This is shown by the lower trace in figure 2*b*. In quantitative work it is therefore necessary to sweep the photomultiplier gain both with and without laser emission, and to take the difference.

4. Chimney plume measurement technique

Two or three years ago giant-pulse ruby lasers were limited to repetition rates of 2 or 3 per minute and displays of the type shown in figure 2 were adequate. The technique for observing chimney plumes consisted of firing a series of shots at various elevation angles in a vertical plane

intercepting the plume (Hamilton 1966). Successive traces were displaced on a photograph by moving the camera, and the plume was revealed as a region of enhanced scatter. Since the complete scan required about 2 min, it fell far short of an effectively instantaneous plume section. Subsequent improvements in the laser system have led to the present repetition rate of 16 per minute and a scan defining the plume envelope can now often be accomplished in as little as 15 s.

This greatly increased rate of scanning has necessitated the development of new display techniques. The first step was to separate successive traces by displacing them automatically on the oscilloscope as a function of elevation angle, which was quite simply achieved by coupling a potentiometer to the axis of elevation and adding a voltage derived from this to the signal voltage. This technique is suitable when the value of the backscatter is needed with accuracy. If, however, the backscatter is mainly of qualitative interest, as in much chimney plume work, then the incorporation of reliable swept gain opens the way to a more attractive display. In this, the backscatter signal is used to modulate the brightness of the oscilloscope spot while the spot is deflected along an inclined sweep determined by the elevation of the lidar. Echoes defining the positions of chimney plumes can thus be presented directly in coordinates of range and height. A few examples of plume observations obtained with this brightness modulated range-height display appear in figures 4 to 10, plates 1 and 2.

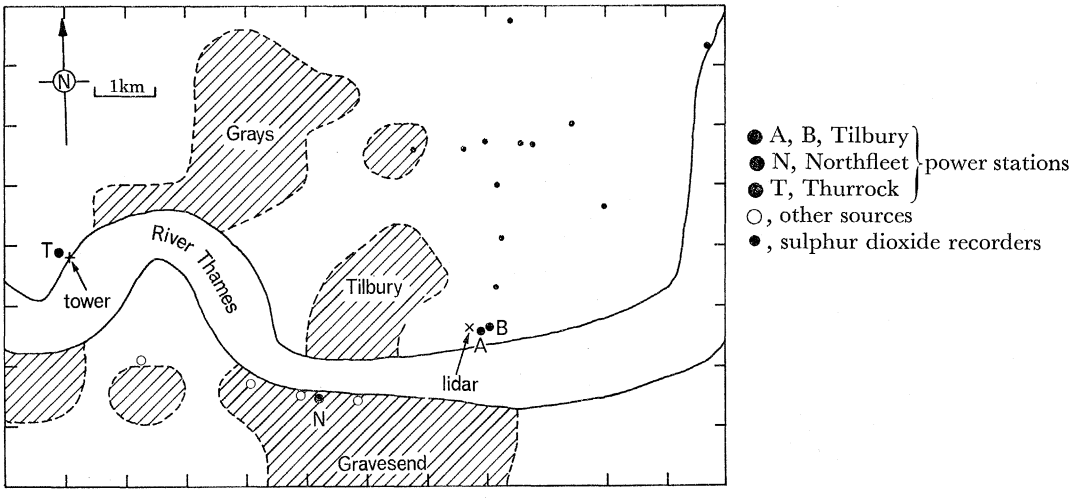

FIGURE 3. Map showing position of lidar in the Central Electricity Generating Board plume dispersion research programme, Tilbury.

Before discussing these examples, it may be of interest to make two technical points. First, the deflexion of the oscilloscope spot at the required inclination to the horizontal was achieved by coupling a sine-cosine potentiometer to the axis of elevation. The oscilloscope time-base sweep was applied to this potentiometer, and components proportional to the cosine and sine of the angle of elevation were derived. These were then applied to the horizontal and vertical plates of the oscilloscope. The other point relates to the modulation of the spot brightness. The signal is applied to the grid of the cathode ray tube in a Tektronix 585 A oscilloscope. Since the variation in brightness is accompanied by a change in spot focus, it might be more accurate to describe the modulation as 'focus modulation'. The backscatter signal can be determined by measuring the width of the oscilloscope trace which is, in fact, a considerable advantage in a low repetition rate lidar where the traces do not overlap. In a high repetition rate system with overlapping

traces focus modulation would be undesirable, and to avoid it might well require the use of an oscilloscope with electromagnetic deflexion.

The examples in figures 4 to 10 should be studied in the light of the map drawn in figure 3 and showing the position of the lidar in relation to the site of the Central Electricity Generating Board (C.E.G.B.) plume dispersion research programme at Tilbury.

In figure 4, plate 1, the lidar scan was on a bearing of 286° and the wind was blowing from 183° at about 9 m s^{-1}. The lidar was thus intercepting plumes from the array of sources along the south bank of the River Thames. The sections are nearly normal to the plume axes and, for the five plumes up to a range of 6 km, were about 2 km downwind of the sources. The plumes from the twin stacks of Thurrock Power Station, at 7 km, were intercepted about 400 m downwind. The conditions under which this observation was made were severe in that the Thurrock Power Station was at the limit of visibility, and the hazy background was bright. Nevertheless, the echo from the Thurrock plume is strong, and it could undoubtedly have been detected much further downwind. Another point of some interest is seen in the two highest traces. These show an abrupt decrease in environmental backscatter at a height of 500 m corresponding to the upper limit of the mixing layer. This is confirmed by the radiosonde ascent made at Crawley (60 km, SW), 4 h earlier, which shows a change from moist air with near-neutral stability to a drier stable layer at just this height. It is often possible to define the mixing layer from the lidar observations in this way.

As well as fixing the position and dimensions of a plume the lidar observation evidently yields some information about the concentration of material in the plume. Thus in figure 4 it is immediately evident from the relative echo intensities that, of the plumes between 2 and 3 km, that at 2.5 km is from the largest plant (Northfleet Power Station) and that at 2 km from the smallest. The pattern of the concentration within a plume may also be revealed by the backscatter. There is yet another measure of concentration available in the form of an extinction measurement. The signal from the environmental aerosol often shows a considerable decrease as the lidar pulse traverses a plume due to the considerable scattering within it. Again referring to figure 4, there has been a sharp decrease in the scatter from beyond the dense Northfleet plume while the weak plume at 2 km caused no perceptible decrease. It can also be seen that the losses were much greater in the upper parts of the Northfleet plume than near the base. The above comments on the interpretation of backscatter measurements are of a qualitative nature and it is naturally desirable to be more quantitative. Without some knowledge of the nature and size of the particles within the plumes, however, it is difficult to interpret the measurements in terms of particle concentrations. It may sometimes be possible usefully to relate different measurements on a single plume, but in many cases this will be made difficult by condensation or evaporation within the plume. A concise survey of the scattering measurements that can usefully contribute to a quantitative knowledge of particulate clouds has been given by Van de Hulst (1957).

On the occasion of figure 5, plate 1, the lidar was directed towards the Northfleet stack. The plume is seen rising as a jet in stable near-calm conditions from its source at 150 m up to a height of more than 600 m. The potential temperature gradient was about 6.0 K km^{-1} throughout the plume's rise and the wind speed about 1 m s^{-1}.

In contrast to this situation, figure 6, plate 1, shows the Northfleet plume blowing towards the lidar on a day of vigorous convective activity. It is distributed throughout the lowest 600 m, and a puff has even reached the surface about 1.5 km downwind. The plume was travelling over the river for this distance, and it is possible that this was a region of persistent downdraught. It is

PHILOSOPHICAL TRANSACTIONS OF THE ROYAL SOCIETY A MATHEMATICAL, PHYSICAL & ENGINEERING SCIENCES

worth commenting on the structure of the plume, which may be described as a string of puffs each with a fairly well defined boundary. The size of the puffs increases and their number decreases with distance downwind. Moore (1966) has drawn attention to this feature of plume structure, which is typical of turbulent conditions.

Another interesting feature evident at a range of 1.5 km is the gap sloping upwards towards the lidar. The lidar scan proceeded upwards in elevation, with successive shots at 10 s intervals. It seems likely that the gap was in fact nearly upright, and that it was recorded obliquely because it was travelling towards the lidar during the scan. If this were so, the rate of travel was 5 m s^{-1}, a figure in agreement with the measured wind speed. It is often possible to deduce the plume speed in this way. The technique can most effectively be exploited by repeated shots at a fixed elevation. Puffs are readily seen progressing along the beam and both their speed and mean height can be measured.

Figure 7, plate 1, shows the two Tilbury power station plumes. The scan is on a bearing of 036° and the plumes are blowing towards 024° (plume A) and 028° (plume B). Plume A is intercepted at a range of 1 km where it has risen from a 100 m stack up to 250 m, while the plume B at 2 km has risen from a 160 m stack up to about 400 m. The wind speed was 7 m s^{-1}. A decrease in the environmental scatter is apparent just below a height of 900 m. That this was the depth of the adiabatic mixing layer was confirmed by the presence of a few wisps of cumulus cloud at this level. The echoes at 1100 m are from the main cloud layer.

The Tilbury plumes are again shown in figure 8, plate 1. On this occasion the plumes were blowing at 6 m s^{-1} over the lidar towards 305°, and the lidar was pointed in the same direction. Plume A has risen by 70 m to 170 m and B by about 200 m to 360 m. The low rise of plume A is accounted for by the presence of a surface inversion, extending almost to a height of 200 m, in which the potential temperature gradient was nearly 30 K km^{-1}. That the plume was in a very stable layer is indicated by its limited depth of about 30 m. Above 200 m the gradient was about 5 K km^{-1} so that the rise of plume B was only slightly, if at all, reduced below its normal neutral rise. Since the plume disperses very little as it travels downwind there is evidently little turbulence in the environment. Nevertheless, it is notable that plume B has broken into puffs, suggesting that this feature of plumes may, at least in part, be due to internal instability.

The last two examples of the brightness-modulated range–height display, in figures 9 and 10, plate 2, demonstrate a useful extension of it. The lidar was directed towards 280° and has intercepted the Northfleet plume, blowing from 205° at 5 m s^{-1}, about 1.8 km downwind of the source. The scan in figure 9 was composed of shots at intervals of 8 s and took about a minute to complete. It shows a plume at a height of 300 m, with a diameter of 300 m and with the disorderly distribution of material characteristic of the instantaneous plume. Figure 10, taken a few minutes later, shows the effect of superimposing six successive 1 min scans. This 6 min mean plume evidently has a much smoother distribution of material. The diameter of the mean plume is almost double that of the instantaneous plume, and the mean height of 400 m shows how unrepresentative was the single observation of figure 9.

The value of 'integrated' scans, like figure 10, is obvious. They can be directly interpreted to give measures of the vertical and lateral dispersion of material, and can be used to obtain accurate measurements of the mean plume height with a minimum of effort. These measurements can then be used to predict the concentration of pollution at the surface. This will form the theme of the next section.

PHILOSOPHICAL TRANSACTIONS OF THE ROYAL SOCIETY A MATHEMATICAL, PHYSICAL & ENGINEERING SCIENCES

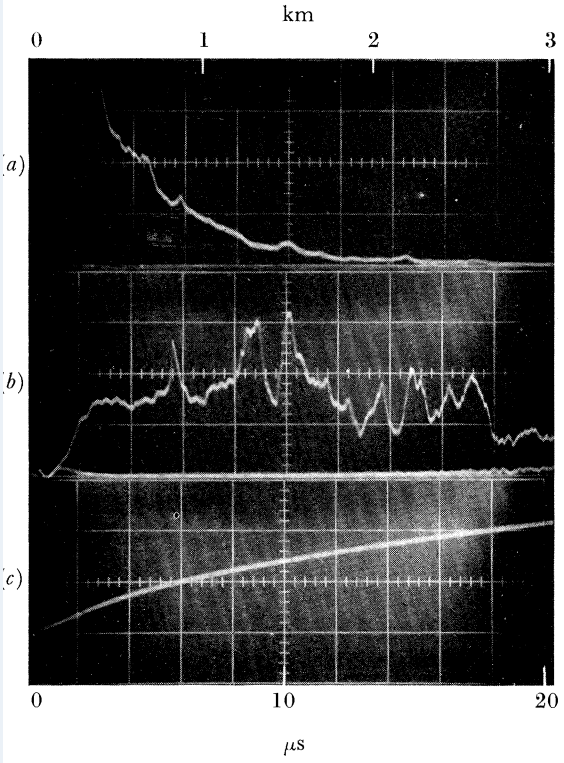

FIGURE 2. Lidar traces of atmospheric backscatter in a light haze. (*a*) Photomultiplier supply 525 V; (*b*), photomultiplier supply swept from 300 to 900 V. (Upper trace shows signal from atmospheric scatter, lower trace that due to background radiance); (*c*), photomultiplier voltage sweep used in (*b*), 300 V per division.

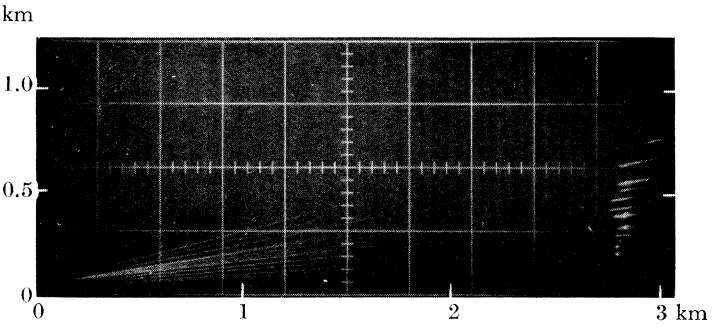

FIGURE 5. Lidar scan, Northfleet plume, 08.16 B.S.T., 11 July 1967. Lidar 247°, wind from 090° at 1 m s^{-1}.

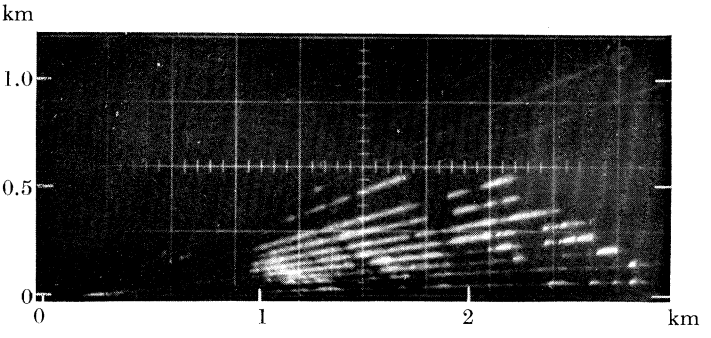

FIGURE 6. Lidar scan, Northfleet plume, 14.32 B.S.T., 13 September 1968. Lidar 247°, wind from 247° at 5 m s^{-1}.

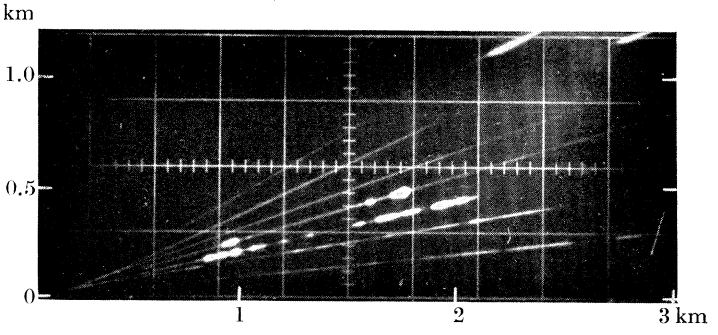

FIGURE 7. Lidar scan, Tilbury plumes, 17.07 B.S.T., 25 September 1968. Lidar 036°, wind from about 026° at 7 m s^{-1}.

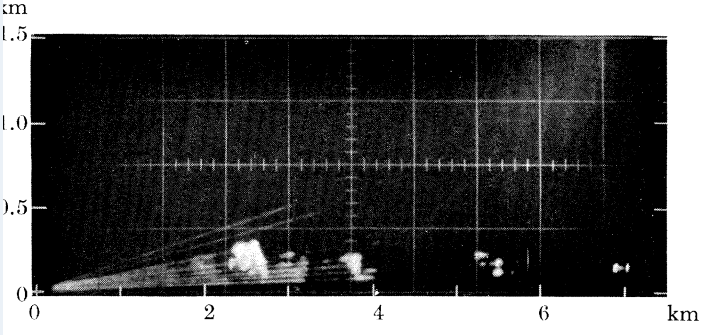

FIGURE 4. Lidar scan, 16.00 B.S.T., 28 October 1968. Lidar 286°, wind from 183° at 9 m s^{-1}.

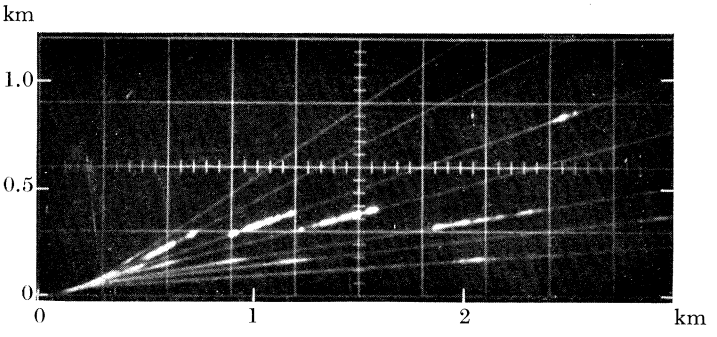

FIGURE 8. Lidar scan, Tilbury plumes, 07.59 B.S.T., 19 September 1968. Lidar 305°, wind from 305° at 6 m s^{-1}.

(*Facing p.* 160)

PHILOSOPHICAL TRANSACTIONS OF THE ROYAL SOCIETY A MATHEMATICAL, PHYSICAL & ENGINEERING SCIENCES

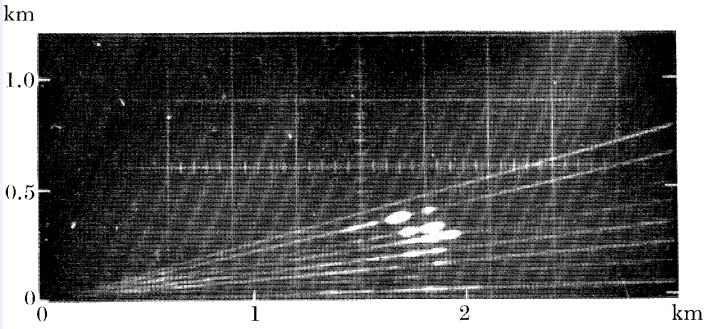

FIGURE 9. Lidar scan, Northfleet plume, 12.12 B.S.T., 25 September 1968. Lidar 280°, wind from 205° at 5 m s^{-1}.

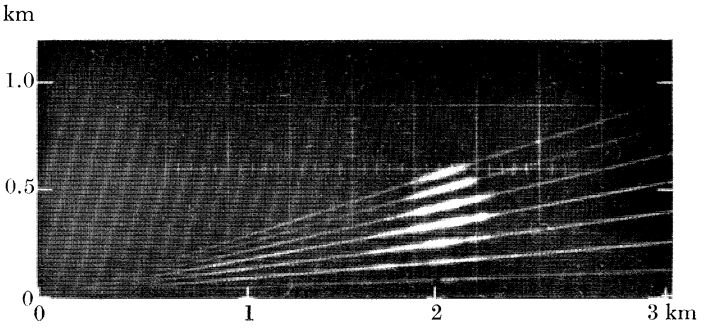

FIGURE 10. Multiple lidar scan, Northfleet plume, six scans, 12.24–12.30 B.S.T., 25 September 1968. Lidar direction and wind as in figure 9.

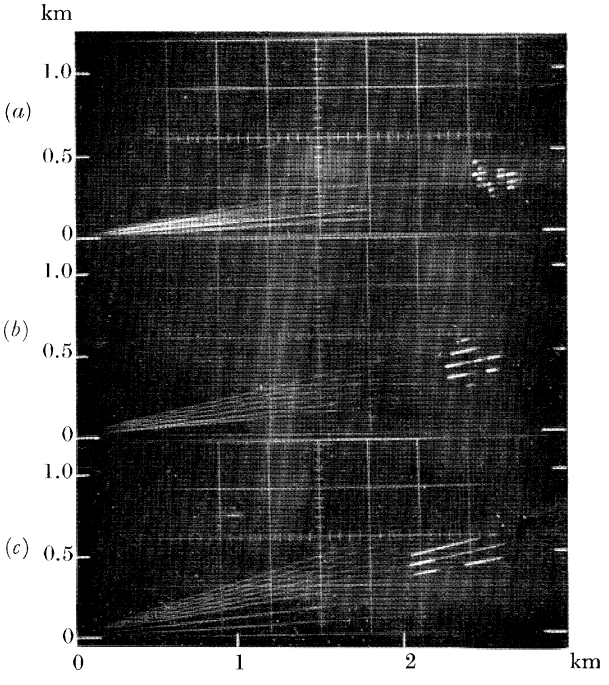

FIGURE 16. Lidar scans, Northfleet plume, 22.15 B.S.T., 5 July 1967. (*a*) Lidar 255°, section 450 m downwind; (*b*), lidar 263°, section 850 m downwind; (*c*), lidar 282°, section 1600 m downwind.

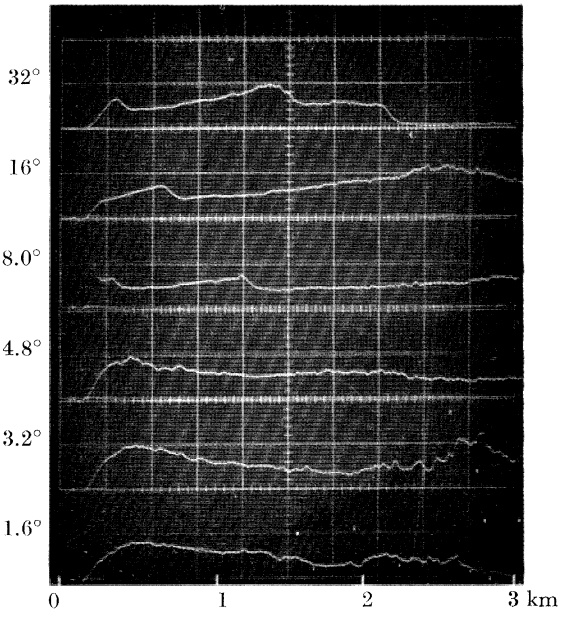

FIGURE 19. Lidar observations of the atmosphere, 19.50 B.S.T., 22 August 1968. Wind from between east and south, light. Lidar direction 000°, elevation of each observation indicated. Visibility 5 km.

PHILOSOPHICAL TRANSACTIONS OF THE ROYAL SOCIETY A MATHEMATICAL, PHYSICAL & ENGINEERING SCIENCES

5. Lidar studies of plume dispersion

The present lidar has been used as part of the Tilbury plume dispersion research programme. The aim of this programme has been to gain a quantitative understanding of the physical processes determining the ground level concentration of pollution downwind of a large elevated source. In the classical treatment of this process (see, for example, Pasquill 1962) it is assumed that the plume disperses from a virtual source at the height to which the plume rises due to its buoyancy and momentum, and that dispersion from this point is such that the distribution of pollution about the plume axis is Gaussian. It can then be shown that the maximum ground level concentration is given by

$$C_{\max} = \frac{2}{e\pi}\frac{Q_S}{uh^2}\left(\frac{\sigma_z}{\sigma_y}\right), \tag{10}$$

where

$C_{\max}$ is the maximum concentration at the ground ($m^3\,m^{-3}$),
Q_S is the source emission ($m^3\,s^{-1}$),
u is the mean wind speed ($m\,s^{-1}$),
h is the virtual source height (m),
σ_y, σ_z are the standard deviations of the horizontal and vertical distributions (m).

This expression is only strictly valid if the ratio σ_z/σ_y does not change with distance, though it is still quite close to the truth if the ratio changes only slowly. The maximum can be shown to occur at the point where

$$\sigma_z = h/\sqrt{2}. \tag{11}$$

In this treatment it is important to remember that the values of σ_y and σ_z depend on the sampling time as well as the distance from the source. In the Tilbury programme, sampling times of 3 min and 1 h have been used, and mean values of the ratio σ_z/σ_y for these periods have been estimated from turbulence measurements as 1.0 and 0.5 (Moore 1967). The mean height of the plume in neutral conditions is well represented by the following expression, based on measurements made both as part of the Tilbury programme and at other C.E.G.B. power stations (Lucas 1967):

$$h = h_c + \alpha Q_H^{0.25}/u, \tag{12}$$

where

h is the mean plume height (m),
h_c is the chimney height (m),
Q_H is the heat emission (MW),
α is a source constant ($m^2\,s^{-1}\,MW^{-0.25}$).

At Northfleet Power Station the value of α is $500\,m^2\,s^{-1}\,MW^{-0.25}$ and, because of peculiar local conditions, an effective chimney height of 120 m is adopted rather than the actual height of 150 m (Hamilton 1967).

The maximum concentration may now be evaluated from (10) by using the appropriate value of σ_z/σ_y and a plume height h given by (12). The wind speed u is observed at the Thurrock meteorological tower (figure 3) and the emission quantities Q_S and Q_H may be estimated from data supplied by the power station. Moore (this volume, p. 145) has compared calculations made in this way with the concentrations of sulphur dioxide observed by the network of recorders, part of which is shown in figure 3. The agreement for a sampling period of 1 h was only good at certain wind speeds, but agreement could be obtained at other speeds if the calculated concentrations were adjusted by a factor which varied with the speed.

Although the adjusted calculations are invaluable in assessing long term pollution distributions, the scatter was too great to permit useful prediction on an hour to hour basis. It seemed

likely that some of the scatter might be due to systematic differences of σ_z/σ_y and h from their assumed mean values and, since these quantities can be measured directly by lidar, it seemed worth using lidar observations in an attempt to obtain useful hourly predictions.

Figure 10, plate 2, is an example of a lidar plume observation over a sampling period of 6 min. Similar observations over a period of 1 h would enable one to measure h, σ_z and σ_y which,

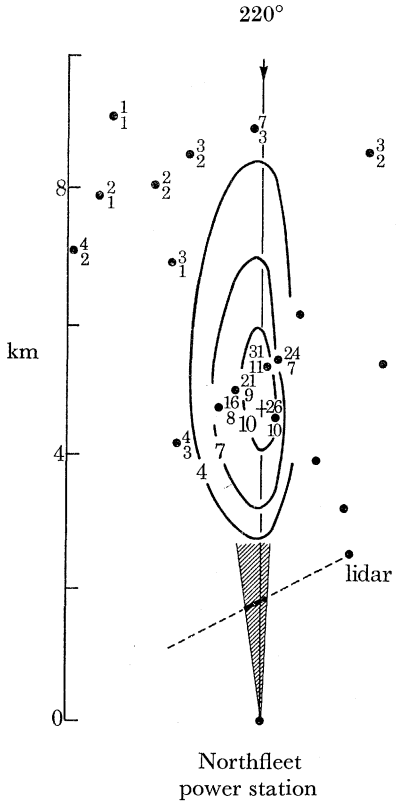

FIGURE 11. Ground level sulphur dioxide concentrations observed 15.30–16.30 B.S.T., 6 May 1966. Recording sites are indicated by spots, lower figure at each site giving the hourly mean concentration, upper figure the 3 min maximum value. Position and direction of lidar scan also shown.

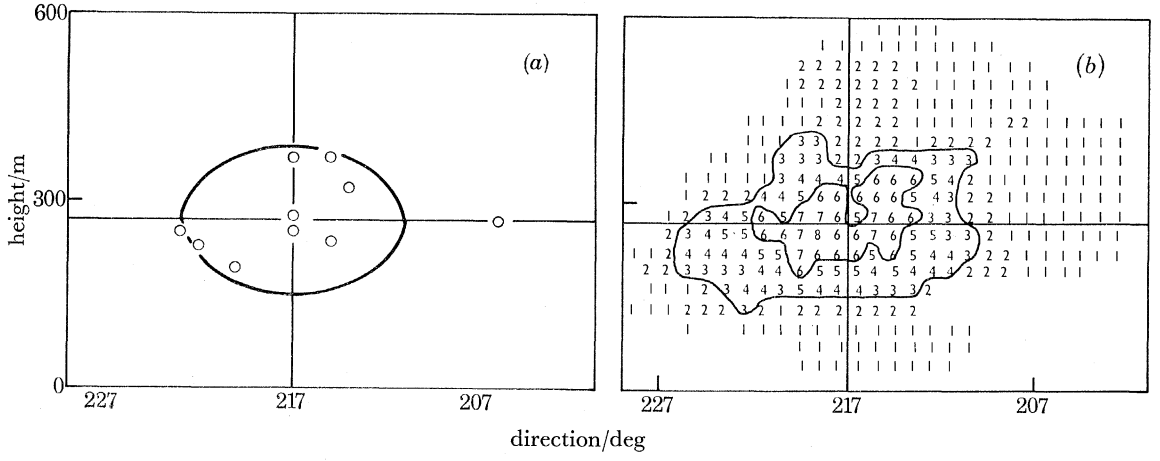

FIGURE 12. Summary of ten lidar scans, 15.30–16.30 B.S.T., 6 May 1966. (*a*) Mean instantaneous size and positions of plume axis; (*b*) number of occasions that each point lay within plume envelope. Contours define regions in which plume was oberved for 30% of occasions (outer) and 60% (inner).

together with the wind speed and emission data, could be used to calculate the maximum hourly concentration. Since these integrated lidar observations have only just become available, however, they have been simulated by combining sequences of nearly instantaneous scans. Figure 11 depicts the situation on an occasion when this has been done. The Northfleet plume was blowing from 220° over the network of recorders. A maximum hourly concentration of about 11 parts/10^8 was recorded just beyond 4 km downwind. The lidar was directed towards 280° and the plume has been intercepted at 1.8 km.

Figure 12 is a summary of the 10 lidar observations made during the hour. The plume's mean instantaneous size is indicated in figure 12*a* together with the positions at which it was observed.

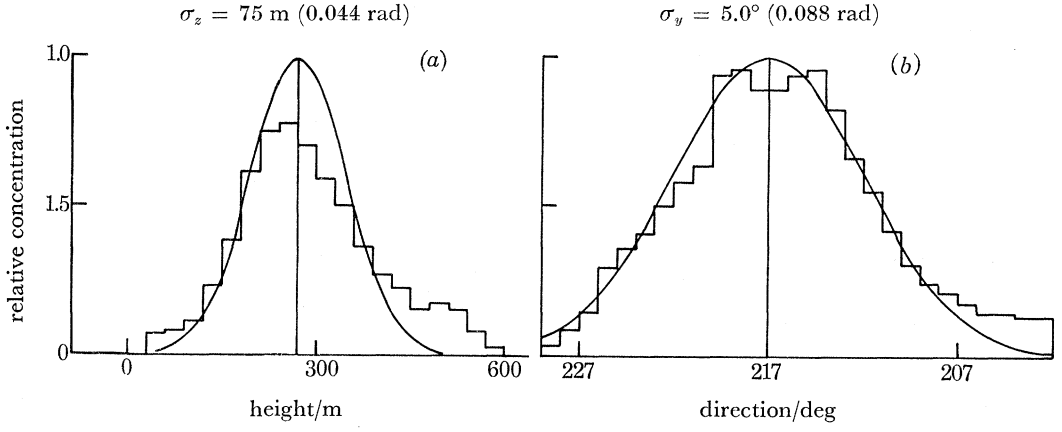

FIGURE 13. Distributions of concentration in plume, 15.30–16.30 B.S.T., 6 May 1966, derived from figure 12. (*a*) Vertical distribution, (*b*) horizontal distribution. Curves represent Gaussian distributions with given standard deviations.

Although the abscissa represents the direction from which the plume has blown, it is to the same scale as the ordinate of height above the ground. The mean size was thus about 300 m horizontally and 200 m vertically. The mean plume height over the hour was 270 m and the mean direction 217°. In figure 12*b* the number of occasions on which the plume was intercepted at each point has been plotted. The contours therefore indicate the plume frequency or, since the concentration in the instantaneous plume appears to be more or less uniform, they may be taken as contours of hourly pollution concentration.

TABLE 3. COMPARISON OF CALCULATED AND MEASURED CONCENTRATIONS OF SULPHUR DIOXIDE

date 1966	time (B.S.T.)	emission $m^3\ s^{-1}$	wind speed $m\ s^{-1}$	mean height/m		vert. s.d./hor. s.d.		max. concn./10^{-8} $m^3\ m^{-3}$		
				lidar	formula	lidar	formula	lidar	formula	observed
4 May	11.00	0.73	8	272	283	0.51	0.50	15	13	17
6 May	11.00	0.56	12	226	221	0.43	0.50	9	11	13
	13.00	0.60	14	237	208	0.37	0.50	7	12	10
	14.00	0.64	14	203	210	0.33	0.50	9	12	11
	15.00	0.67	14	180	211	0.41	0.50	14	13	16
	16.00	0.61	14	270	209	0.50	0.50	7	12	10
	17.00	0.65	12	215	225	0.47	0.50	13	13	15
	18.00	0.68	11	250	236	0.67	0.50	15	13	18
13 May	17.00	0.33	8	285	254	0.63	0.50	7	7	10
14 May	15.00	0.43	9	285	247	0.61	0.50	8	9	12
	16.00	0.43	9	298	247	0.79	0.50	10	9	11
19 May	21.00	0.52	12	177	219	0.35	0.50	11	11	14

It is interesting to compare the distribution of figure 12 with a Gaussian distribution and this has been done in figure 13. For convenience, the values of the standard deviation for the two Gaussian curves were calculated by combining one quarter of the mean instantaneous spread with the standard deviation of the position measurements, assuming that the variance of the total distribution was equal to the sum of the variances of the components. The horizontal distribution in figure 13*b* is evidently close to the Gaussian. The vertical distribution in figure 13*a* is somewhat

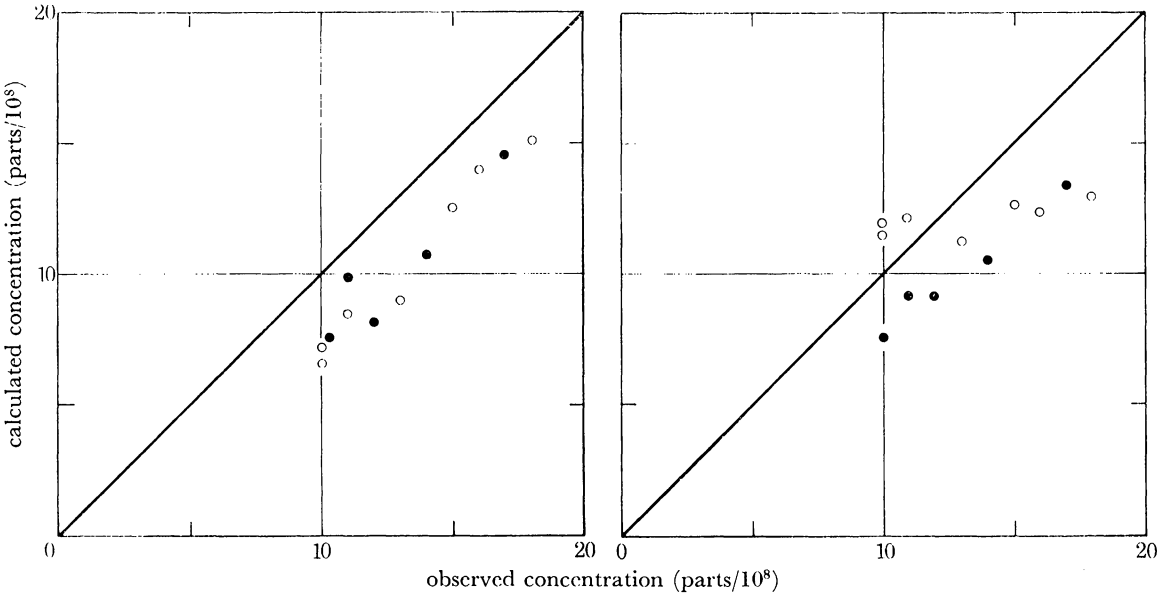

FIGURE 14. Comparison of calculated and observed ground level maximum sulphur dioxide concentrations. ○, periods on 6 May 1966; ●, other occasions. Calculations based on lidar observations of plume height and spread.

FIGURE 15. Same as figure 14, but calculations based on estimated values of plume height and spread.

different, showing evidence of rather more effective dispersion above the plume axis than below it. However, the Gaussian shown is a good fit to the distribution below the axis and should therefore be appropriate for predicting surface concentrations.

As explained earlier, the values of plume height and the ratio σ_z/σ_y can be measured from the lidar observations of figure 12 and used in equation (10) to calculate the maximum ground level concentration. On this occasion the wind speed was 14 m s^{-1} and the sulphur dioxide emission was 0.61 m^3 s^{-1} (at s.t.p.), leading to a predicted concentration of 7 parts/10^8. This should be compared with the observed value of 10 parts/10^8, taken as the value shown in figure 11 reduced by the 1 part/10^8 attributable to background pollution. Similar calculations have been performed for a total of 12 periods and are summarized in table 3 and figure 14. For comparison, the results of calculations using equation (12) for the plume rise and a value of 0.50 for the ratio σ_z/σ_y are also tabulated, and they appear graphically in figure 15.

The periods shown were 0.5 to 1.0 h long though, since just over half were 1 h long, the average was 0.9 h. The number of lidar scans in each period ranged from 6 to 12 with an average of 9. The occasions chosen have also been restricted to conditions of near neutral atmospheric stability. Under these conditions, the lidar-based calculations of figure 14 are evidently well correlated with the observed concentrations, though they do appear to be consistently about 3 to 4 parts/10^8

lower. It is possible that this is due to significant contributions to the measured concentrations from other industrial sources near the power station, but the discrepancy is hardly more than the experimental error.

At first sight, the formula-based calculations of figure 15 are also quite close to the observed values, although the correlation is evidently not quite so good. Closer scrutiny, however, shows up an interesting difference. Since a fixed value of 0.50 was taken for σ_z/σ_y in the formula calculations, the meteorological variability only entered equation (10) through the term uh^2. However, because h was calculated from equation (12) and is inversely dependent on u, the term uh^2 varied very little over the range of table 3. The variation in the calculated concentrations of figure 15 is therefore almost entirely due to variations in the rate of emission, Q_S. Thus, for the set of seven nearly consecutive periods on 6 May 1966, because Q_S was almost constant, there was little variation in the calculated concentrations. On the other hand, the measured concentration varied over a range of almost a factor two, a variation that appears to have been closely reproduced in the lidar-based calculations.

A closer look at the factors contributing to this variation on 6 May is instructive. The ratio σ_z/σ_y ranged from 0.33 to 0.67 with a geometric mean of 0.45 while uh^2 varied from 0.45×10^5 to $1.0 \times 10^5\,\mathrm{m^3\,s^{-1}}$ with a mean of $0.65 \times 10^5\,\mathrm{m^3\,s^{-1}}$. These mean values are close to the values in the formula-based calculations of 0.50 for σ_z/σ_y and an effectively constant $0.60 \times 10^5\,\mathrm{m^3\,s^{-1}}$ for uh^2. In fact, each of the quantities σ_z/σ_y and uh^2 ranged over a factor of 2, and the reason that the calculated concentration was limited to just about the same range of variation appears to be that σ_z/σ_y and uh^2 were negatively correlated. In the light of these variations in the basic parameters, the correlation between the calculated concentrations and the measured values is evidently good.

On the basis of this small sample it seems that useful predictions can be made from lidar observations from hour to hour. However, two limitations should be stressed. A comparison tried over a few periods of stable conditions gave very poor results. On these occasions the value of σ_z/σ_y measured 2 km downwind was obviously not a reasonable estimate of the value at the distance of maximum ground level concentration. The other limitation is that the period should not be less than 0.5 h in duration, at any rate for a measuring network whose resolution is no better than the present one (recorder separation less than 5°). For periods less than this it was not generally possible to relate the surface pattern to the lidar observations. Short term predictions will probably have to be developed statistically from measurements over a longer period.

6. Lidar studies of plume rise

It is evident that lidar is well suited to the study of plume rise. Because of its great sensitivity it can detect the plume well downwind of the source under a very wide range of meteorological conditions. An earlier study, based on lidar measurements, related the rise of the Northfleet plume 1.5 km from the chimney to the heat emission, wind speed and atmospheric stability (Hamilton 1967). Such studies are useful in supplying practical information for the design of new plant, but measurements at a fixed distance cannot really be used in testing the various models of plume rise. For this purpose, measurements are needed to define the plume trajectory and, in this section, an example of such measurements is presented and analysed.

In several theoretical treatments of plume rise, the rate of change of the upward momentum of a plume element is equated to its buoyancy. A further assumption is that processes are adiabatic.

The following outline is based on Moore's (1966) treatment. The two basic equations of momentum and heat conservation may be written

$$u^2 \frac{\mathrm{d}}{\mathrm{d}x}\left(V\frac{\mathrm{d}z}{\mathrm{d}x}\right) = V\left(\frac{\theta-\theta_e}{\theta}\right)g \tag{13}$$

and

$$\frac{\mathrm{d}}{\mathrm{d}x}(V) = \theta_e \frac{\mathrm{d}V}{\mathrm{d}x}, \tag{14}$$

where

V is the volume of a plume element (m^3),
θ is the potential temperature of the element (K),
θ_e is the potential temperature of the environment (K),
z is the height of the element (m),
x is the distance of the element from the source (m),
u is the wind speed ($m\,s^{-1}$),
g is the acceleration due to gravity ($m\,s^{-2}$).

In conditions of neutral stability, the solution of these equations is given by

$$\frac{V}{x_P}\frac{\mathrm{d}z}{\mathrm{d}x} = x_M^2 + x_B x, \tag{15}$$

where

x_P is the length of the plume element (m),
$x_M = F_M^{\frac{1}{2}} u^{-1}$ is a momentum length (m),
$x_B = F_B u^{-3}$ is a buoyancy length (m),
F_B is the flux of buoyancy at the source ($m^4\,s^{-3}$),
F_M is the flux of momentum at the source ($m^4\,s^{-2}$).

As Moore has pointed out, it is implicit in this treatment that the momentum and heat are uniformly distributed throughout the element. However, provided the actual distributions remain similar throughout the rise and growth of the element, any non-uniformity may be accounted for by including a constant factor in (13) and hence (15).

The plume trajectory can be calculated from (15) if V and x_P are known as functions of x or z. The various plume rise models assume different analytical forms for these functions. However, with lidar observations, it is possible to measure V and x_P and to test the equation numerically. A suitable occasion on which this could be done occurred on 5 July 1967.

On this occasion, conditions were very steady with a light wind of $5\,m\,s^{-1}$, and the plume trajectory changed little over a period of an hour or more. A developing radiation inversion extended up to a height of 150 m and, above this, the tower measurements indicated a neutral layer up to 300 m. Radiosonde measurements 3 h later suggested that this neutral layer continued to about 600 m with a potential temperature gradient of $3\,K\,km^{-1}$ from that height to 1400 m. The stable surface layer evidently served to insulate the upper neutral layer from the surface and, consequently, the plume was rising in a layer of low turbulence. The plume was blowing from 190° and scans were made through the plume at 450, 850 and 1600 m downwind by directing the lidar towards 255, 263 and 282° respectively. The sections were therefore nearly normal to the plume axis. One of the sequences is shown in figure 16, plate 2. On this occasion the Northfleet power station emission was restricted to just one of the two chimneys. The break apparent in the middle of the plume sections, particularly that nearest to the source, is evidence of a bifurcated plume. This plume is an example of a cylindrical thermal of the type described by Richards (1963). The model appropriate on this occasion is that described by Moore as a

continuous plume. It should be stressed that our observations indicate that this type of plume is not, in fact, of common occurrence, but it has been chosen because the relevant measurements can be made much more easily and the analysis is relatively simple. The measurements of rise and spread are summarized in figure 17. These represent the average of three scans at each of the three distances from the source.

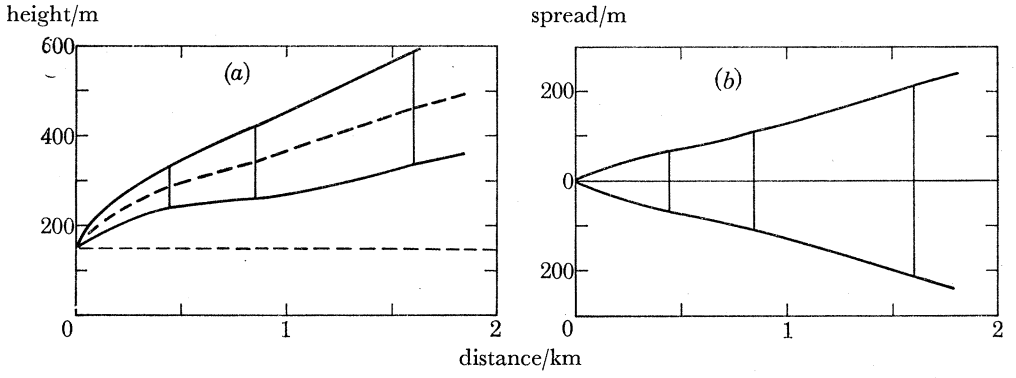

FIGURE 17. Northfleet plume, 21.30–21.40 B.S.T., 5 July 1967.
(*a*) Rise and vertical spread; (*b*) horizontal spread.

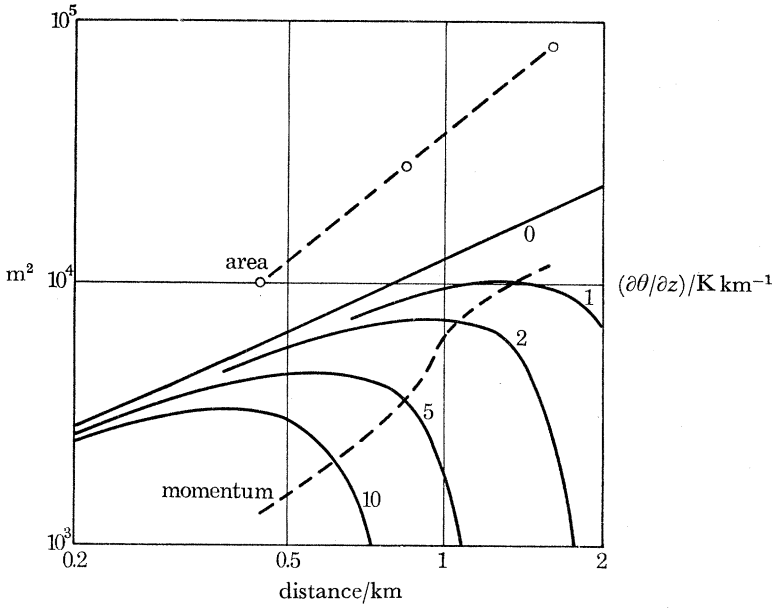

FIGURE 18. Comparison of observed plume momentum and theoretically deduced momentum for the plume in figure 17. Solid lines give theoretical values for various potential temperature gradients $\partial\theta/\partial z$ (K km^{-1}). Broken lines give plume cross-sectional area and observed momentum.

In the case of a continuous plume the volume of a plume element is given by $V = Ax_{\mathrm{P}}$, where A is the plume cross-sectional area (m²). Equation (15) thus reduces to

$$A\,\mathrm{d}z/\mathrm{d}x = x_{\mathrm{M}}^2 + x_{\mathrm{B}}x. \tag{16}$$

The left hand side of this equation, which essentially represents the upward momentum of a plume element of unit length, can be determined from figure 17. The right hand side, representing the sum of the initial momentum and that arising from the action of the buoyancy force, is deduced from the station emission data and the wind speed. On the occasion of these observa-

tions, the volume emission was the equivalent of $450\,m^3\,s^{-1}$ at the environmental temperature and pressure. The efflux velocity was about $20\,m\,s^{-1}$ and the temperature of emission 100 K above ambient. Thus $F_M = 9 \times 10^3\,m^4\,s^{-2}$ and $F_B = 1.5 \times 10^3\,m^4\,s^{-3}$, whence $x_B = 12\,m$ and $x_M^2 = 360\,m^2$. For these values, the right hand side has been evaluated and is shown in figure 18 as the uppermost member of the family of solid lines. The measured values of A and $A\,dz/dx$ are also shown, by the broken lines.

It can be seen that $A\,dz/dx$ is only a fraction of $x_M^2 + x_B x$. This fraction increases from 0.25 at 450 m to 0.60 at 1600 m. As mentioned earlier, one likely reason for the need of an adjustment factor in (16) is the non-uniformity in the distribution of heat and momentum within a plume element. In fact, the plume on this occasion was probably well represented by a vortex-pair model (Richards 1963). The vertical momentum of the plume must really be determined by integration over the entire volume of the upward moving fluid, including that outside the plume element. Richards found, however, that the velocity distribution of a thermal remained similar throughout its growth. If this is true of the plume, then the apparent momentum appearing on the left hand side of (16) is a fixed fraction of the true momentum, and the model can still be used with an appropriate adjustment factor. The measurements of 5 July 1967 indicate that the apparent momentum is of the order of 0.25 to 0.60 of the true value. The factor can also be calculated from data provided by Richards for his model thermals. In five experiments the values were 0.44, 0.71, 0.39, 0.37 and 0.44.

Although the mean value of the presently observed factor agrees reasonably well with Richards's values, it is difficult to account for the systematic increase. If conditions were not neutral then the right hand side of (16) would be modified. The solid curves in figure 18 show the modified values for different positive potential temperature gradients. It is most unlikely that the actual gradient exceeded 1 or 2 K km^{-1} in the layer up to a height of 600 m. Such a gradient would not significantly affect the plume until beyond 800 m and then it would, of course, have the effect of reducing the adjustment factor. A more likely possibility is that there was systematic vertical motion in the plume environment. Certainly, there is some evidence that, in moderate winds at least, the Northfleet plume is depressed by about 30 m as it travels from the south bank over the river. It is presumably possible that upward motion could occur as it travels over the north bank. This kind of behaviour would have contributed to a change in the adjustment factor of the form observed. However, a full explanation would require further study.

Tentatively, then, equation (16) can be used to determine the trajectory of a continuous plume, provided the right hand side is multiplied by a factor whose value is around 0.5. It should be emphasized that this factor may well be different for other, perhaps more common, types of plume. Although this conclusion may be tentative, the foregoing analysis does indicate the great contribution that lidar can make to an understanding of plume rise.

7. Lidar studies of the mixing layer

A commonly observed feature of the lower atmosphere is the existence of a well defined adiabatic layer extending from the surface up to the base of a stable layer. Pollution emitted into the adiabatic layer ultimately mixes throughout its depth, while that emitted into the stable layer may disperse only slowly with little or, perhaps, none of it reaching the mixing layer below. The depth of this mixing layer is clearly a major factor in determining ground level concentrations of pollution and the measurement of it is therefore of great importance in pollution studies.

PHILOSOPHICAL TRANSACTIONS OF THE ROYAL SOCIETY A MATHEMATICAL, PHYSICAL & ENGINEERING SCIENCES

Lidar observations are frequently able to provide just this measurement. The top of the mixing layer is usually revealed by a sharp decrease in the lidar backscatter, as for example, in figures 4 and 7, plate 1. Further examples have been discussed by Barrett & Ben-Dov (1967) and Hamilton (1966).

The value of swept gain in opening the way to brightness modulated range–height displays for chimney plume studies was emphasized in § 3. It is, however, equally valuable in facilitating a ready evaluation of lidar observations of the mixing layer, as may be seen from the example of figure 19, plate 2. This shows the atmospheric scatter observed at a series of angles of elevation at 19.50 B.S.T. on 22 August 1968. It was an occasion of anticyclonic conditions, with a light south-easterly air stream. The figure shows the situation at sunset.

Sharp decreases in the backscatter are immediately seen at several levels. On the probe made at 32° elevation they occur at heights of 200, 800 and 1150 m, and at 8° yet another is seen at 50 m. Tower and radiosonde measurements confirmed that there was a developing radiation inversion extending up to 200 m, with a shallow adiabatic mixing layer in the bottom 50 m. The base of the subsidence inversion, indicating the daytime mixing layer, was at 1300 m at Crawley (60 km, SW) and 800 m at Hemsby (150 km, NE). The reason for this difference was presumably that before reaching Crawley the air had passed over land for some 60 km, while at Hemsby it had passed over the sea. The fact that the lidar observations reveal discontinuities at both levels suggests that the air at Tilbury was of mixed origin, that below 800 m having travelled over the Thames estuary from the east while that above had travelled over land from the south. This pattern would have been the result of a sea breeze circulation superimposed on the general south-easterly flow. It is confirmed by the observation during the day of small cumulus clouds moving from the south and dissipating as they reached the easterly air stream blowing up the estuary.

The main dispersive characteristics can usually be established from a qualitative study of the lidar observations. The measurements of received power, can, however, also be analysed to provide estimates of the aerosol concentration, as has been done by Barrett & Ben-Dov (1967). They have shown that the aerosol concentration is proportional to the volume backscattering coefficient for a wide range of aerosol distributions. Unfortunately, because of the effects of extinction, the lidar does not measure the true volume backscattering coefficient directly but, rather, a quantity that may be termed the apparent backscattering coefficient, β'_a, given by

$$\beta'_a(r) = \beta'(r) \exp\left[-2\int_0^r \sigma(r')\,\mathrm{d}r'\right]. \tag{17}$$

However, if the extinction and backscattering coefficients are related by an expression of the form

$$\sigma = C(\beta')^\alpha,$$

where C and α are constants, then (17) can be inverted by a method originally due to Hitschfeld & Bordan (1954) to give

$$\beta'(r) = \beta'_a(r)\left\{1 - 2\alpha C\int_0^r [\beta'_a(r')]^\alpha\,\mathrm{d}r'\right\}^{-1/\alpha}. \tag{19}$$

As Hitschfeld & Bordan pointed out, a practical difficulty attending the use of this equation is that accurate results can only be achieved if the constant C and the system sensitivity are known with great precision. Even if nature were cooperative in providing a precise value of C, Hitschfeld & Bordan showed that, in the case of radar, it was entirely impracticable to establish the system sensitivity with anything like the required precision. On the other hand, they went on to show

that if, in addition to measurements of the apparent backscatter, one did have knowledge of the true backscatter at some distant point then one could immediately use (19) to determine the true backscatter at all intermediate distances. This principle can be applied to lidar measurements.

The measurements shown in figure 19, plate 2, clearly show evidence of considerable horizontal uniformity, and it is possible to take advantage of this fact in a correction procedure. The technique is simply to compare the results of various trial corrections in which α and C are varied and to adopt that which gives the greatest horizontal consistency. This has been done for the measurements of 22 August 1968 and the resulting vertical profiles of corrected backscatter are shown in figure 20. On this occasion, α was actually taken to be unity and a value of $C = 2.7$

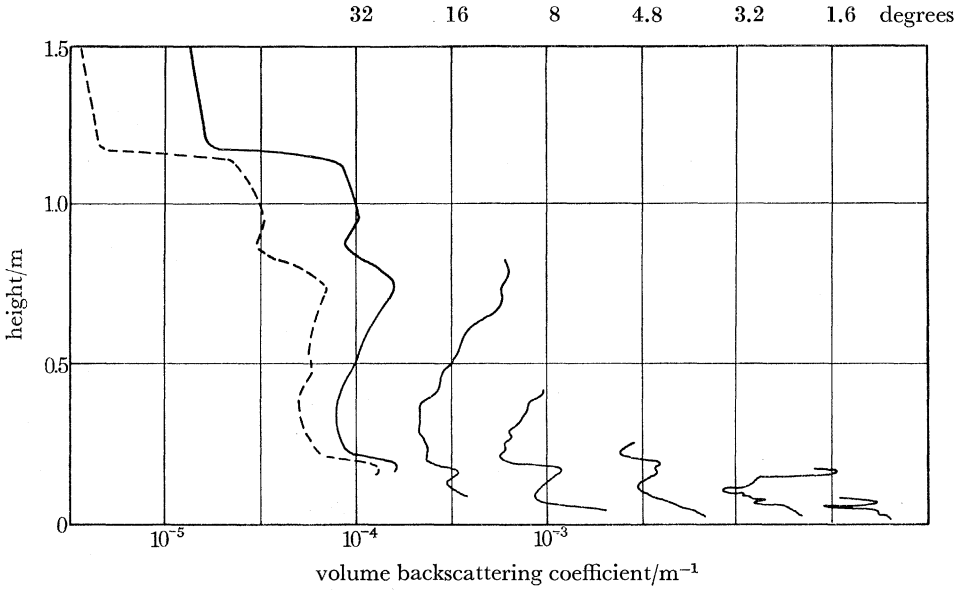

FIGURE 20. Vertical profiles of the volume backscattering coefficient, 19.50 B.S.T., 22 August 1968. Solid lines show values corrected for extinction. Broken line shows uncorrected profile observed at elevation 32°. The abscissa scale applies to the observation at 32°, the other observations having been displaced to the right by successive intervals of $10^{0.5}$.

then appeared to give the greatest consistency. For comparison, the profile of apparent backscatter has also been included for the observation at an elevation of 32°, showing that the extinction had reduced the backscatter at 1500 m to one quarter of its true value. It can now be seen that, overall, the aerosol concentration was fairly uniform below 1150 m, but there was a strong tendency for the concentration to be less than the mean at the bottom of each distinctive layer and greater at the top.

It is interesting to note that, on this occasion, the swept gain had been adjusted to correct for the inverse square law reduction plus an additional 7 dB extinction over the range from 300 m to 3 km. Since the aerosol was fairly uniform, this adjustment gave a very good first order correction, and the traces of figure 19 are good representations of the true backscatter. In practice, the swept gain can often be adjusted to give good overall correction in this way, but for quantitative work, the full analysis outlined above must be followed. The full correction procedure has actually been simulated electronically by Wein (1961) for a weather radar. The same technique could be used for lidar, though, because the final choice of correction must in practice be determined subjectively, it may be better done after the event rather than in real time.

Even though the swept gain can only be used for a qualitative correction it is worth reiterating that its essential contribution is to the accuracy of the measurements. On 22 August 1968 it enabled the backscatter to be measured with almost the same accuracy at all ranges. Without it, the accuracy of the measurements at 3 km would have been reduced by more than two orders of magnitude. It is clear that swept gain is almost essential for quantitative work of the type that has been outlined in this section.

8. Conclusions

Lidar evidently has a valuable part to play in the study of chimney plumes. The plumes from large industrial plant can usually be detected some kilometres from their source and at a distance of several kilometres from the lidar. The way in which swept gain can be used to provide uniform sensitivity with distance has been described. This has opened the way to both the development of a brightness modulated display and the accurate measurement of the backscatter coefficient over a wide range of distances.

Observations of the plume made over a period of about an hour can be used to predict ground level concentrations of pollution. In neutral conditions, these predictions appear to be significantly better than those made purely on the basis of meteorological measurements. The analysis of the lidar observations on which these predictions are based is greatly facilitated by making a time exposure of the brightness modulated display over the period of interest. The relevant measurements can be made directly from this.

Lidar has also been used to study the trajectory of the plume during its rise. A fairly simple model can be used to predict this trajectory if the rate of growth of the plume is known. In this model, the rate of change of upward momentum of a plume element is taken to be equal to the buoyancy force. A lidar case study has suggested that the model can be used, but that the momentum change must be equated to a fraction (about one-half) rather than the whole of the buoyancy force. This, in turn, suggests that the true momentum is somewhat greater than that deduced from observation of the visible element.

Finally it has been shown that lidar observations of the environment in which plumes rise and disperse often reveal details of its structure that are vital to an appreciation of the behaviour of the plumes. A technique of analysis was outlined whereby it is possible to obtain vertical profiles of the aerosol concentration in the lower layers.

In conclusion, it may not be too much of an exaggeration to say that lidar is the most valuable single tool currently available for the study of chimney plumes.

This work is part of the study of air pollution by the Central Electricity Research Laboratories, and the paper is published by permission of the Central Electricity Generating Board. Thanks are also due to Mr I. Kerenyi, formerly of G. and E. Bradley, Ltd, for his persistence in developing a reliable swept gain unit.

References (Hamilton)

Barrett, E. W. & Ben-Dov. O. 1967 Application of the lidar to air pollution measurements. *J. appl. Met.* **6**, 500–515.
Cohen, V. 1968 Gain correction in laser rangefinders. *Electron. Engng* **40**, 260–262.
Collis, R. T. H. 1966 Lidar: a new atmospheric probe. *Q. Jl R. met. Soc.* **92**, 220–230.
Foitzik, L. & Zschaeck, H. 1953 Messungen der spektralen Zerstreuungsfunktion bodennaher Luft bei guter Sicht, Dunst und Nebel. *Z. Met.* **7**, 1–19.
Hamilton, P. M. 1966 The use of lidar in air pollution studies. *Int. J. Air Wat. Pollut.* **10**, 427–434.

Hamilton, P. M. 1967 Plume height measurements at Northfleet and Tilbury power stations. *Atmos. Environment* **1**, 379–387.

Hitschfeld, W. & Bordan, J. 1954 Errors inherent in radar measurement of rainfall at attenuating wavelengths. *J. Met.* **11**, 58–67.

Kaplan, R. A. & Daly R. T. 1967 Performance limits and design procedure for all-weather terrestrial range-finders. *IEEE J. Quantum Electron. QE*–3, 428–435.

Lucas, D. H. 1967 Application and evaluation of results of the Tilbury plume rise and dispersion experiment. *Atmos. Environment* **1**, 421–424.

Middleton, W. E. K. 1952 *Vision through the atmosphere.* University of Toronto Press.

Moore, D. J. 1966 Physical aspects of plume models. *Int. J. Air Wat. Pollut.* **10**, 411–417.

Moore, D. J. 1967 Meteorological measurements on a 187 metre tower. *Atmos. Environment* **1**, 367–377.

Northend, C. A., Honey, R. C. & Evans W. E. 1966 Laser radar (Lidar) for meteorological observations. *Rev. scient. Instrum.* **37**, 393–400.

Pasquill, F. 1962 *Atmospheric diffusion.* London: D. Van Nostrand.

Richards, J. M. 1963 Experiments on the motions of isolated cylindrical thermals through unstratified surroundings. *Int. J. Air Wat. Pollut.* **7**, 17–34.

Twomey, S. & Howell, H. B. 1965 Relative merits of white and monochromatic light for the determination of visibility by backscattering measurements. *Appl. Opt.* **4**, 501–506.

Van de Hulst, H. C. 1957 *Light scattering by small particles.* New York: Wiley.

Waldram, J. M. 1945 Measurement of the photometric properties of the upper atmosphere. *Q Jl R. met. Soc.* **71**, 319–336.

Waldram, J. M. 1945*b* Measurement of the photometric properties of the upper atmosphere. *Trans. illum. Engng Soc.* **10**, 147–188.

Wein, M. 1961 The electronic correction for attenuation of 3.2 cm radar signals from rain. *Proc. Ninth Weather Radar Conf. Am. Met. Soc.* pp. 367–370.

PHILOSOPHICAL TRANSACTIONS OF THE ROYAL SOCIETY A MATHEMATICAL, PHYSICAL & ENGINEERING SCIENCES

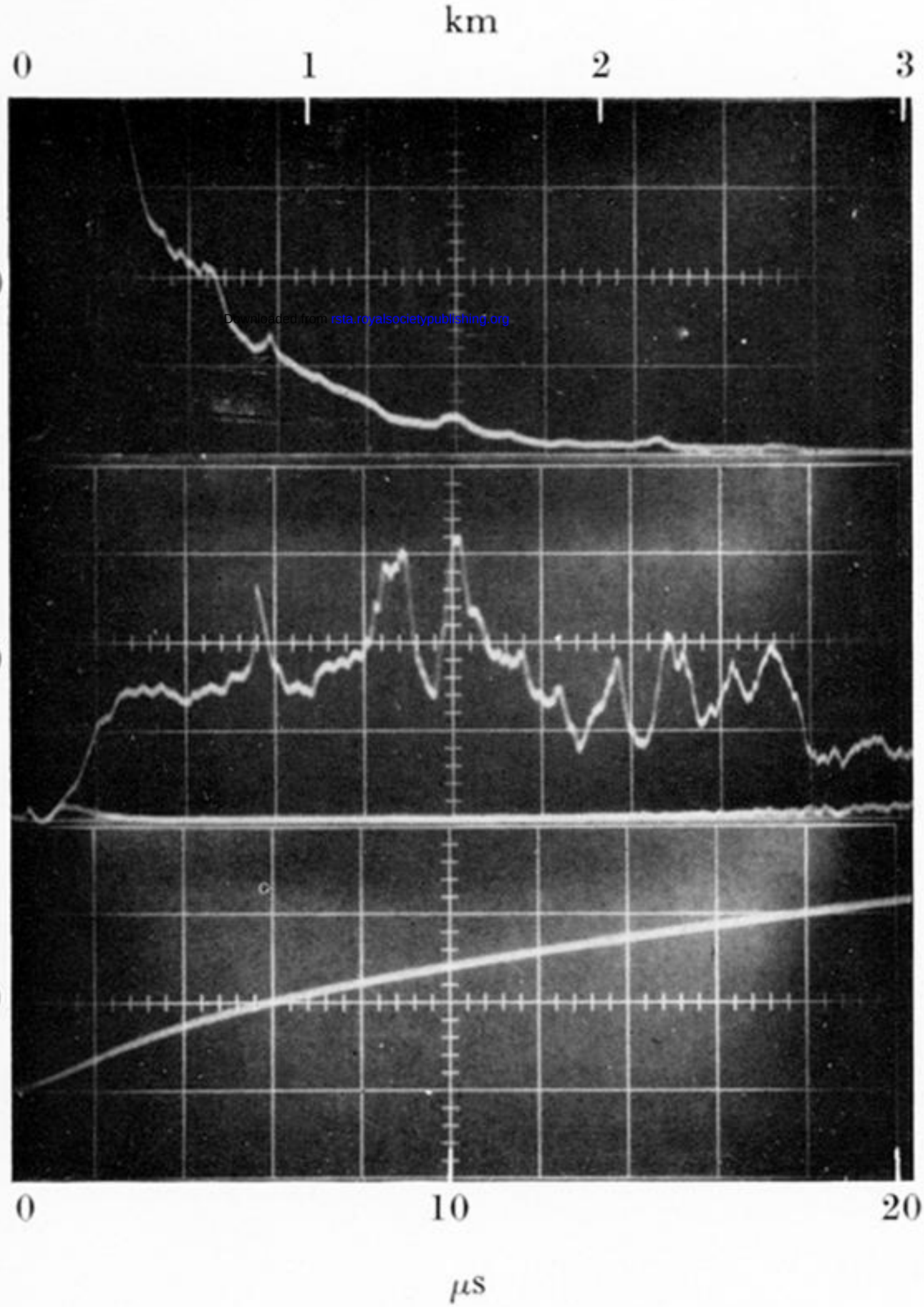

PHILOSOPHICAL TRANSACTIONS OF THE ROYAL SOCIETY A MATHEMATICAL, PHYSICAL & ENGINEERING SCIENCES

FIGURE 2. Lidar traces of atmospheric backscatter in a light haze. (*a*) Photomultiplier supply 525 V; (*b*), photomultiplier supply swept from 300 to 900 V. (Upper trace shows signal from atmospheric scatter, lower trace that due to background radiance); (*c*), photomultiplier voltage sweep used in (*b*), 300 V per division.

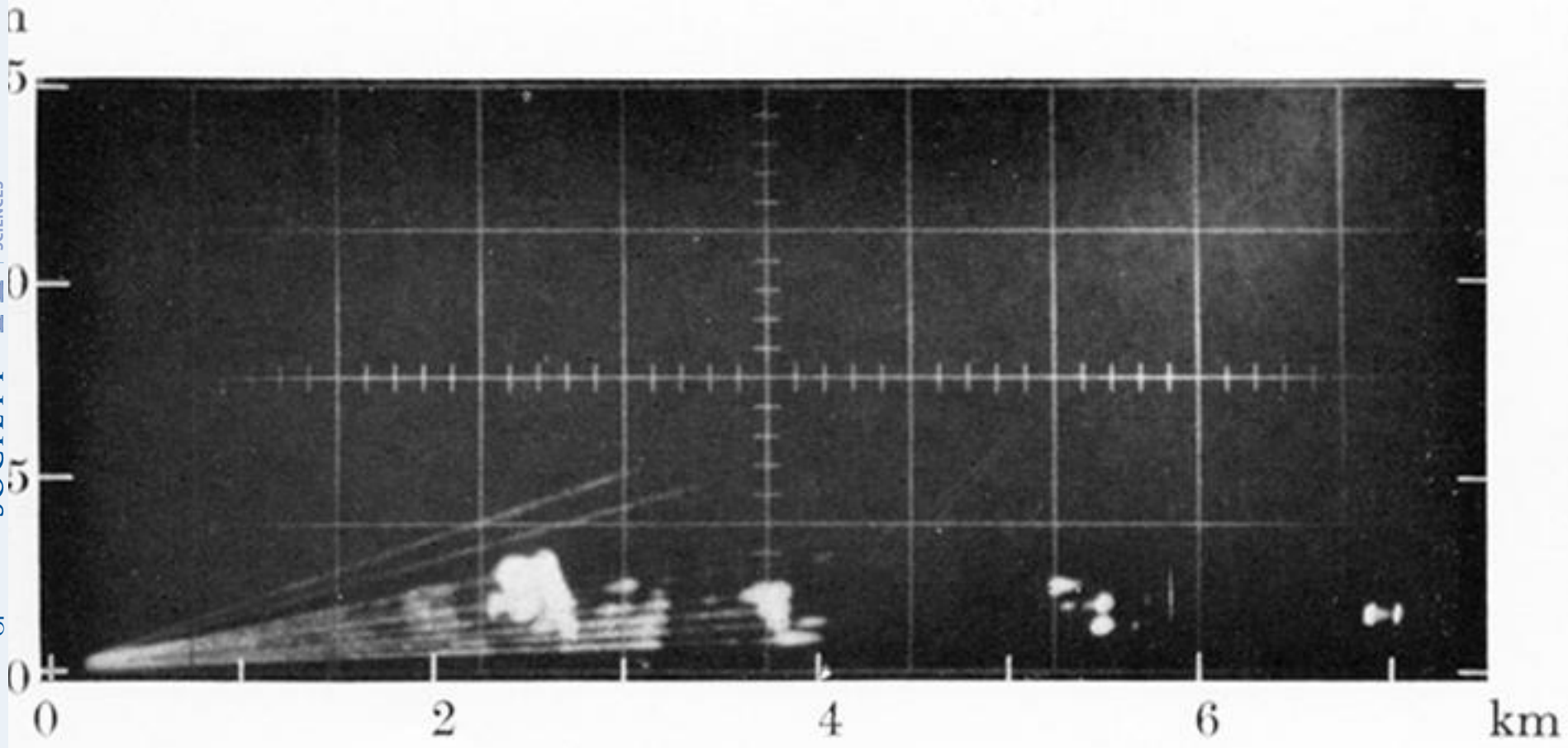

FIGURE 4. Lidar scan, 16.00 B.S.T., 28 October 1968. Lidar 286°, wind from 183° at 9 m s^{-1}.

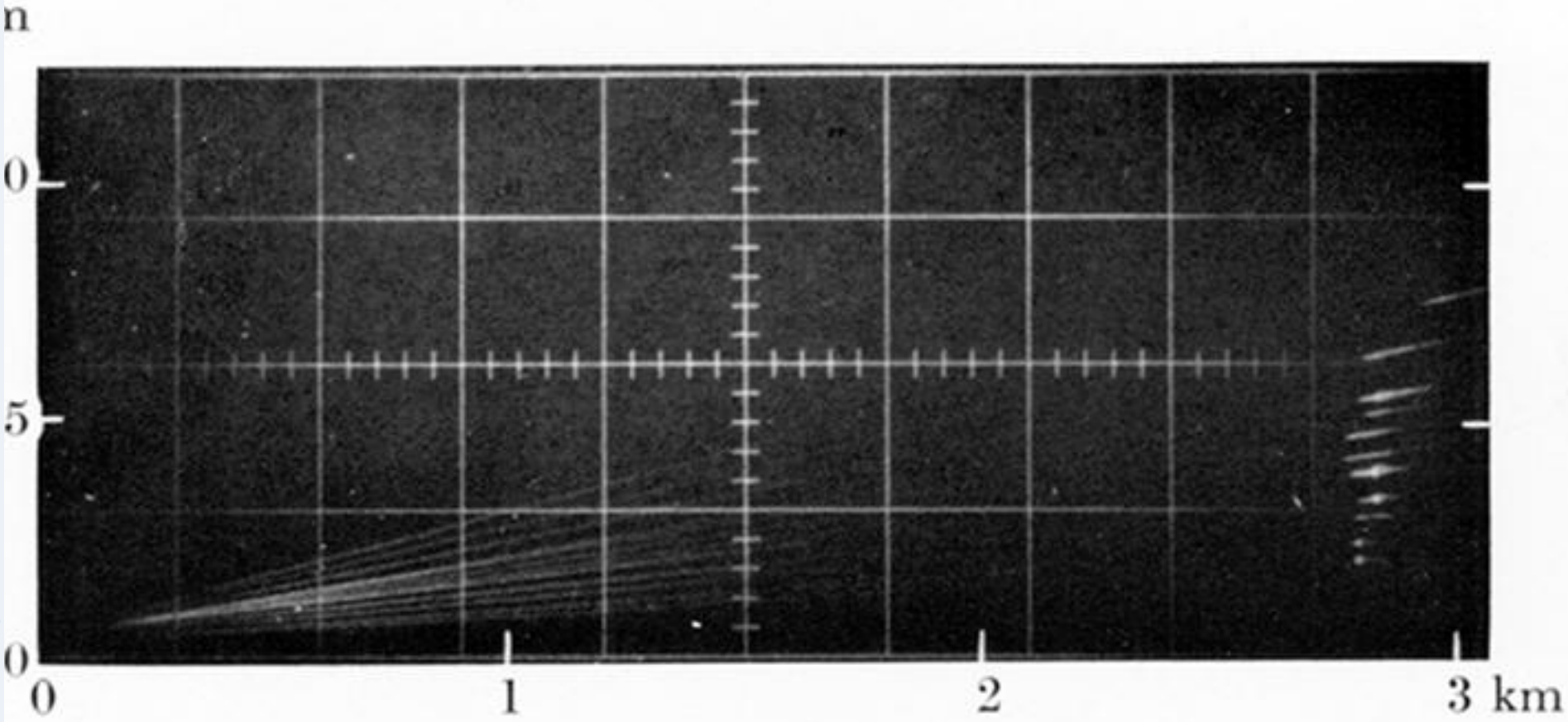

FIGURE 5. Lidar scan, Northfleet plume, 08.16 B.S.T., 11 July 1967. Lidar 247°, wind from 090° at 1 m s^{-1}.

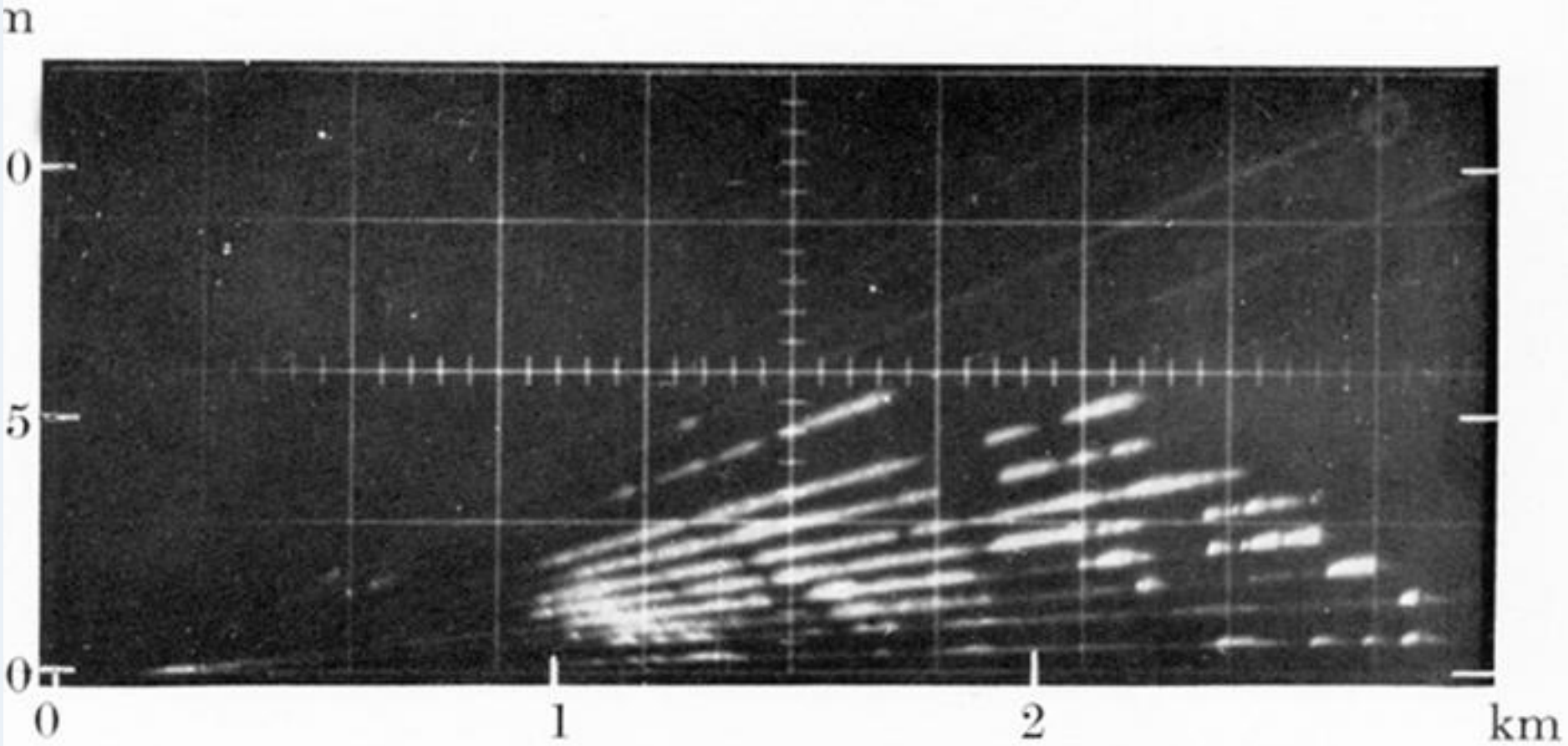

FIGURE 6. Lidar scan, Northfleet plume, 14.32 B.S.T., 13 September 1968. Lidar 247°, wind from 247° at 5 m s^{-1}.

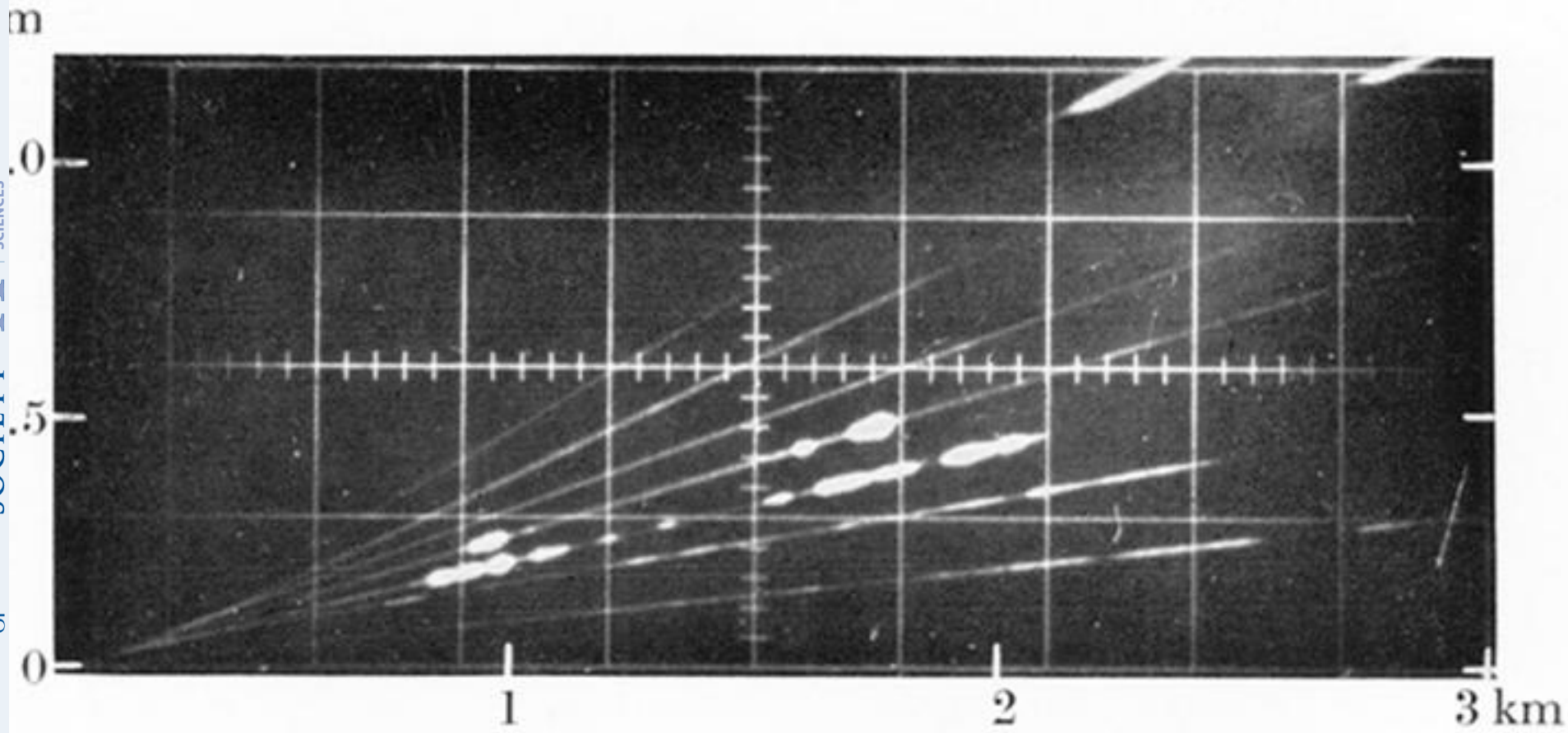

FIGURE 7. Lidar scan, Tilbury plumes, 17.07 B.S.T., 25 September 1968. Lidar 036°, wind from about 026° at 7 m s^{-1}.

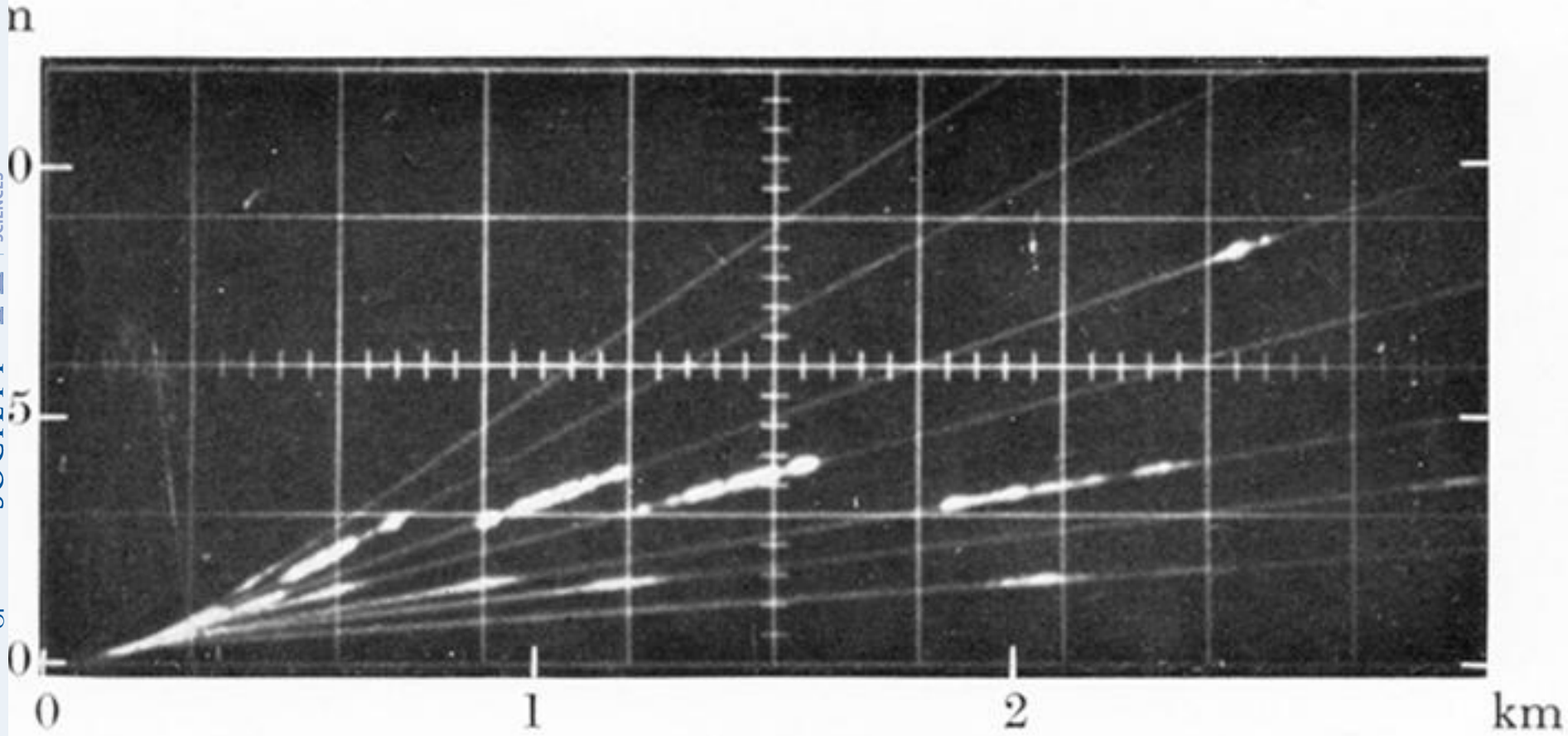

FIGURE 8. Lidar scan, Tilbury plumes, 07.59 B.S.T., 19 September 1968. Lidar 305°, wind from 305° at 6 m s^{-1}.

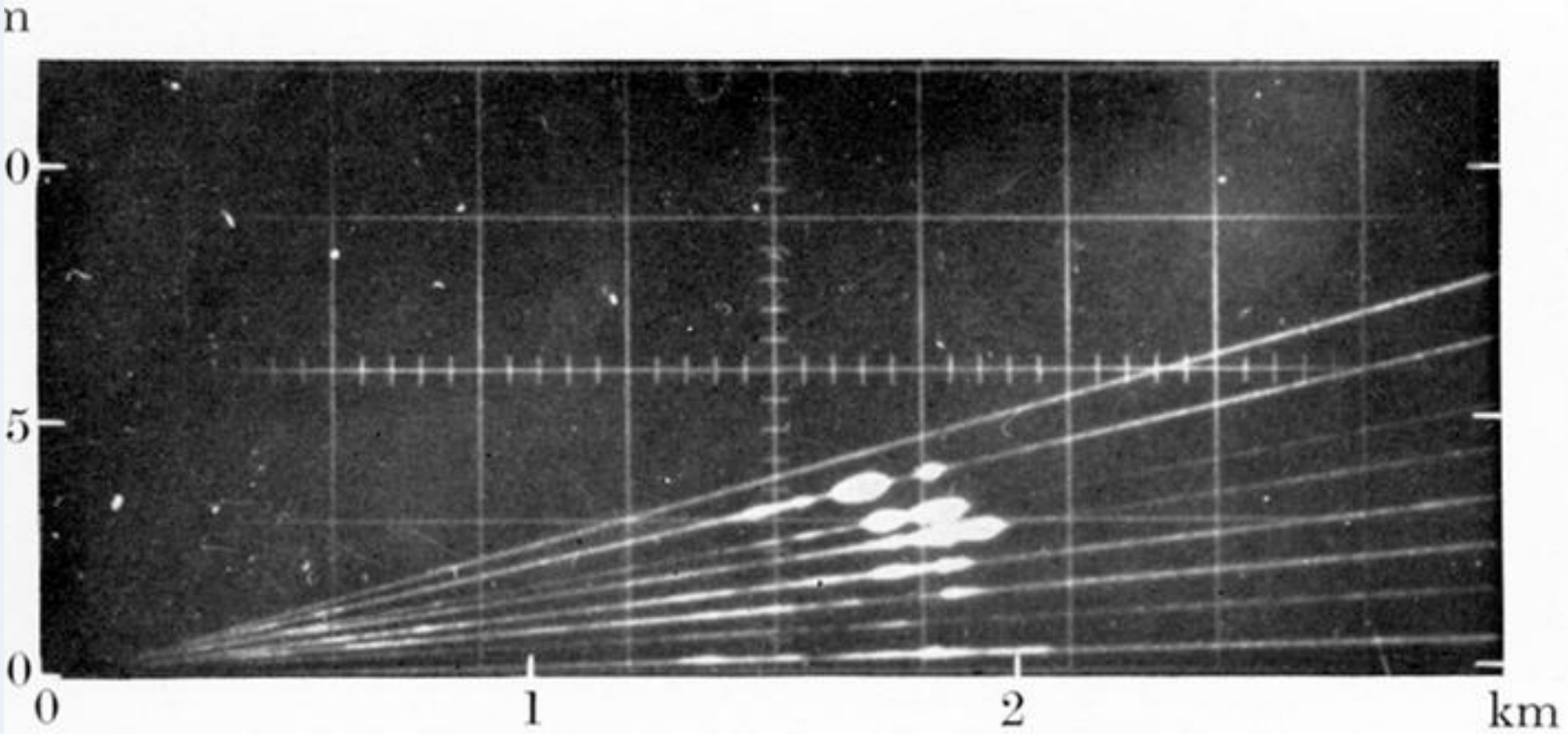

FIGURE 9. Lidar scan, Northfleet plume, 12.12 B.S.T., 25 September 1968. Lidar 280°, wind from 205° at 5 m s^{-1}.

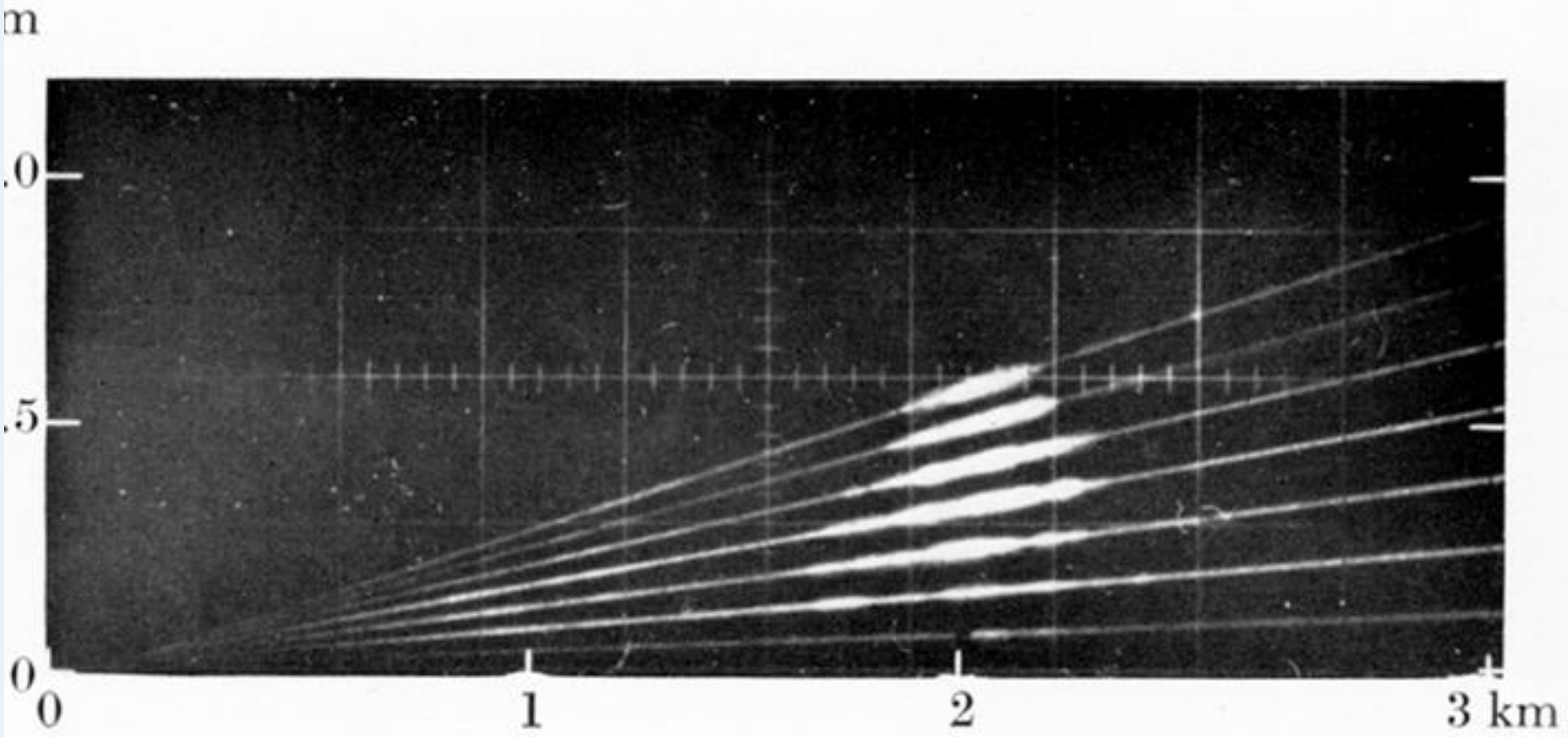

FIGURE 10. Multiple lidar scan, Northfleet plume, six scans, 12.24–12.30 B.S.T., 25 September 1968. Lidar direction and wind as in figure 9.

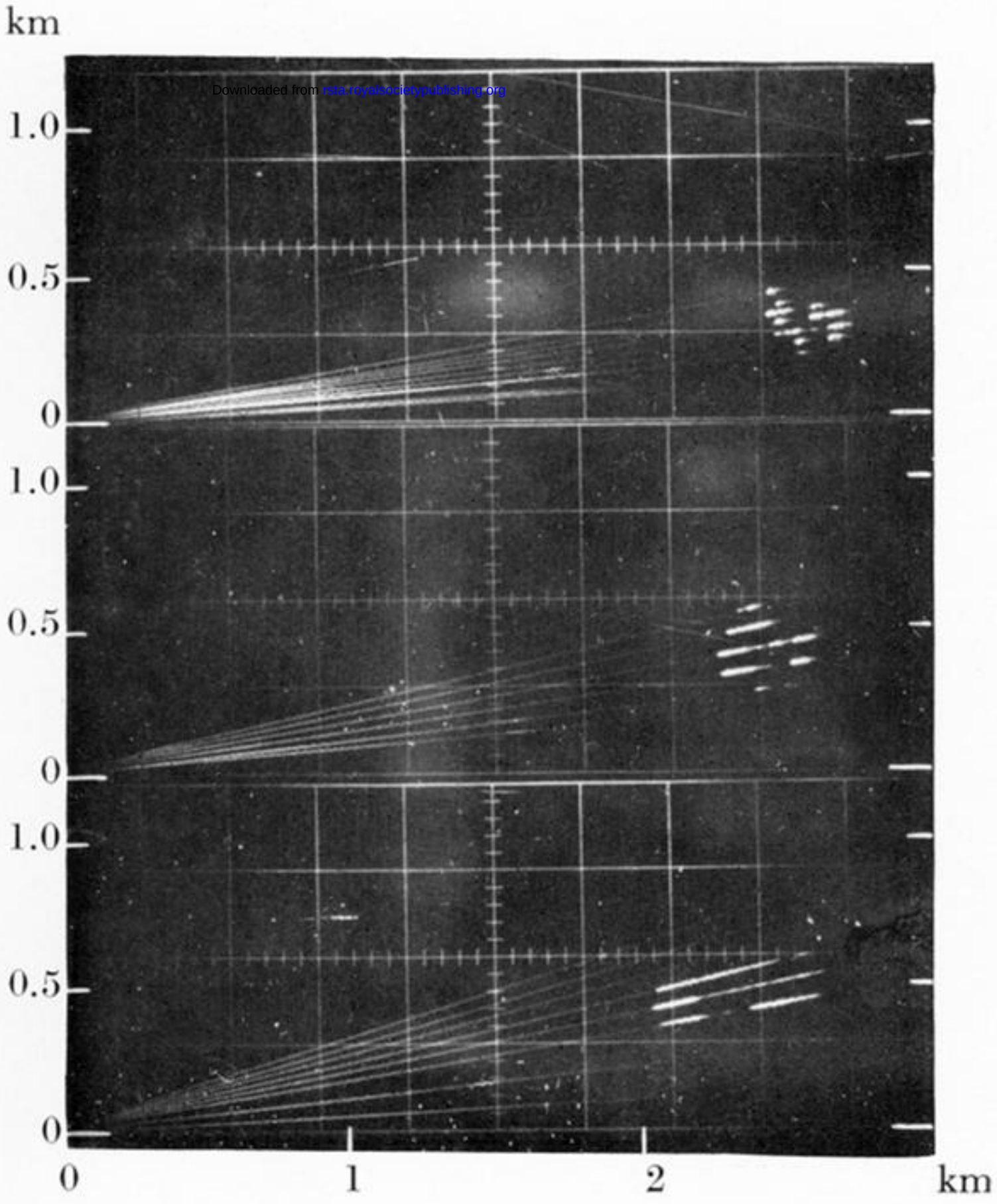

FIGURE 16. Lidar scans, Northfleet plume, 22.15 B.S.T., 5 July 1967. (*a*) Lidar 255°, section 450 m downwind; (*b*), lidar 263°, section 850 m downwind; (*c*), lidar 282°, section 1600 m downwind.

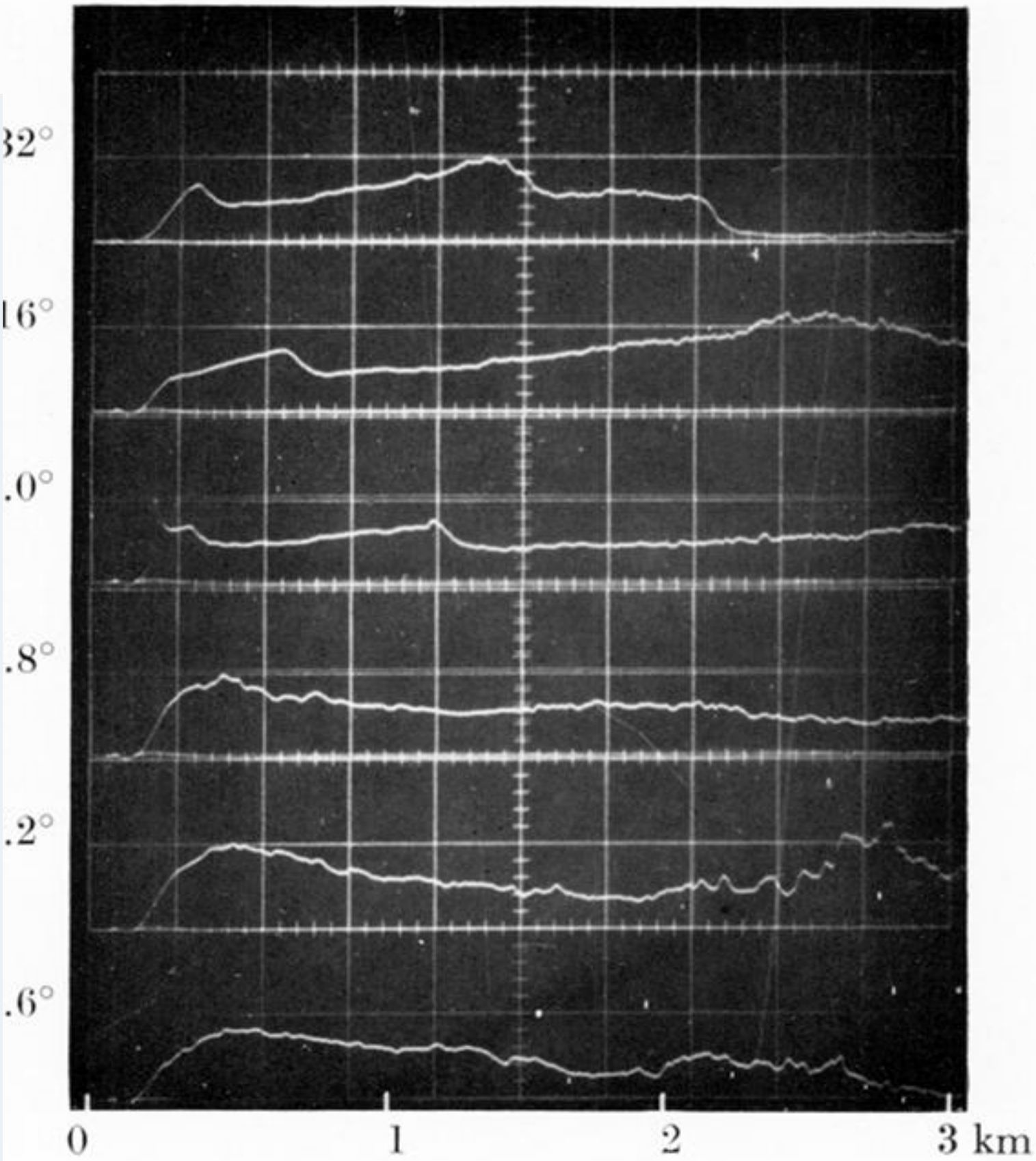

FIGURE 19. Lidar observations of the atmosphere, 19.50 B.S.T., 22 August 1968. Wind from between east and south, light. Lidar direction 000°, elevation of each observation indicated. Visibility 5 km.

PHILOSOPHICAL TRANSACTIONS OF THE ROYAL SOCIETY A MATHEMATICAL, PHYSICAL & ENGINEERING SCIENCES